Shallow water table effects on water, sediment and pesticide transport in vegetative filter strips: Part A. non-uniform infiltration and soil water redistribution

R. Muñoz-Carpena[1], C. Lauvernet[2], N. Carluer[2]

[1]University of Florida, Department of Agricultural and Biological Engineering, PO Box 110570, Gainesville, FL 32611-0570, USA

[2]Irstea, UR MALY, centre de Lyon-Villeurbanne, F-69626 Villeurbanne, France

Correspondence to: R. Muñoz-Carpena (carpena@ufl.edu)

Abstract. Vegetation buffers like vegetative filter strips (VFS) are often used to protect water bodies from surface runoff pollution from disturbed areas. Their typical placement in floodplains often results in the presence of a seasonal shallow water table (WT) that can decrease soil infiltration and increase surface pollutant transport during a rainfall/runoff event. Simple and robust components of hydrological models are needed to analyse the impacts of WT in the landscape. To simulate VFS infiltration under realistic rainfall conditions with WT, we propose a generic infiltration solution (Shallow Water table INfiltration algorithm: SWINGO) based on a combination of approaches by Salvucci and Entekhabi (1995) and Chu (1997) with new integral formulae to calculate singular times (time of ponding, shift time, and time to soil profile saturation). The algorithm was tested successfully on 5 distinct soils both against Richards's numerical solution and experimental data in terms of infiltration and soil moisture redistribution predictions, and applied to study the combined effects of varying WT depth, soil type, and rainfall intensity and duration. The results show the robustness of the algorithm and its ability to handle various soil hydraulic functions, and initial non-ponding conditions under unsteady rainfall. The effect of a WT on infiltration under ponded conditions was found effectively decoupled from surface infiltration/excess runoff processes for depths larger than 1.2 to 2 m, shallower for fine soils and shorter events. For non-ponded initial conditions, the influence of WT depth also varies with rainfall intensity. Also, we observed that soils with a marked air entry (bubbling pressure) exhibit a distinct behaviour with WT near the surface. The good performance, robustess and flexibility of SWINGO supports its broader use to study WT effects on surface runoff, infiltration, flooding, transport, ecological and land use processes. Coupling with an existing VFS model in the companion paper (Lauvernet and Muñoz-Carpena, 2017), where the potential effects of seasonal or permanent WTs on VFS sediment and pesticide trapping are studied.

1 Introduction

The use of vegetative filter strips (VFS) can reduce sediment and surface runoff pollutants (i.e. sediment, colloids, nutrients, pesticides, pathogens) movement into receiving water bodies. The dense vegetation/soil system reduces runoff pollutants in three ways by increasing: a) soil infiltration that reduces total runoff volume (and dissolved runoff pollutants); b) surface roughness that reduces surface velocity and produces settling of sediment and sediment-bonded pollutants; c) contact between dissolved and particulate pollutants with the soil and vegetation surfaces that enhances their removal from runoff (Muscutt et al., 1993; Muñoz-Carpena et al., 1999; Dosskey, 2001; Fox et al., 2010; Muñoz-Carpena et al., 2010; Yu et al., 2013; Lambretchs et al., 2014; Wu et al., 2014). The efficiency of VFS in trapping pollutants is heavily influenced by the highly variable spatial and temporal dynamics introduced by site-specific combinations of soil, climate, vegetation, and human land use. For the case of runoff pesticides, these influences have been recognised in multiple field studies (Lacas et al., 2005; Reichenberger et al., 2007; Poletika et al., 2009; Sabbagh et al., 2009). Other effects like hydraulic loading under concentrated flow conditions (Fox et al., 2010) or timing of the pesticide application (Sabbagh et al., 2013) can also result in reduced filter trapping efficiencies. As these systems are complex, the practice of using generic, simple regression equations relating the reduction efficiency of pollutants with VFS physical characteristics (i.e. length, slope) is often inadequate (Fox and Sabbagh, 2009).

Mechanistic understanding of VFS behaviour has advanced significantly in the last 20 years and numerical simulation tools are available to analyse this important best management practice (BMP) under upland field conditions where runoff is governed by excess rainfall and field inflow processes (Muñoz-Carpena et al., 1993, 1999; Abu-Zreig, 2001; Muñoz-Carpena and Parsons, 2004; Poletika et al., 2009; Sabbagh et al., 2009; Carluer et al., 2017). A recent linked mechanistic model has investigated multiple input factors and their relative importance and uncertainties of on the predicted reduction of runoff, sediments, and pesticides (Fox et al., 2010; Lambrechts et al., 2014; Muñoz-Carpena et al., 2010, 2015).

However, because of their location near or at the riparian zone, VFS can at times be bounded by a seasonal shallow water table (WT) (Borin et al., 2004; Ohliger and Schulz, 2010). Examples of ubiquitous areas where these conditions exist either seasonally or on a more permanent basis are humid coastal flatland zones, floodplains near water bodies, and soils with limiting horizons resulting in perched WTs. Generally, capillary effects from a WT can reduce infiltration and increase subsequent runoff processes, and have a major effect on contaminant transport to surface waters (Gillham, 1984). In spite of the potentially important environmental impacts of the presence of shallow water under VFS, there is a dearth of studies addressing this problem either experimentally or mechanistically. Several authors suggest the importance of this factor in VFS experimental studies (Lacas et al., 2005; Arora et al., 2010) or when designing or implementing this field BMP (Simpkins et al., 2002; Dosskey et al., 2006, 2011), but they do not provide a mechanistic interpretation. Some authors suggest that the reduction of infiltration and VFS efficiency can be problematic for seasonal WT depths above 2 m typical of hydromorphic soils (Dosskey et al., 2006, 2011; Lacas et al., 2012). As cited by Salvucci and Entekhabi (1995), the importance of accounting for areas of WT effects in water balance and runoff studies has been recognized for a long time and specialized analysis and simulation approaches have been proposed

by numerous authors (for example, Vachaud et al. 1974; Srivastava and Yeh, 1991; Salvucci and Entekhabi, 1995; Chu, 1997; Basha, 2000).

In spite of the ubiquity and importance of these areas and previous specialized analysis and modelling efforts, commonly used field and watershed hydrological models are limited when describing infiltration and soil water redistribution with WT (Beven, 1997, Liu et al., 2011). Among existing simulation approaches, solutions to the fundamental Richards (1931) partial differential equation (RE) can describe the infiltration and redistribution of water in soil, including the specific case of when a system contains a WT. However, RE does not have a general analytical solution and its application real-world systems requires computationally intensive numerical approximations that can result in mass-balance and instability errors in some cases (e.g. for coarse soils and highly dynamic boundary conditions) (Celia et al., 1990; Paniconi and Putti, 1994; Miller et al., 1998; Vogel et al., 2001; Ross, 2003; Seibert et al., 2003). As a result, soil infiltration is often modelled in field and watershed models using simpler physically-based approaches (Jury et al., 1991; Smith et al., 1993; Haan et al., 1994; Singh and Woolhiser, 2002; Talbot and Ogden, 2008; Ogden et al., 2015). One of the most often used approaches in hydrologic modelling is the Green-Ampt (1911) model adjusted to account for variable rainfall (Mein and Larson, 1973; Chu, 1978; Skaggs and Khaleel, 1982). The model has the advantages of being computationally efficient and that its parameters can be directly estimated from physical measurements, or derived indirectly from soil texture (Rawls et al., 1982, 1983). However, the limitation of the original Green–Ampt model is that it assumes isotropic soil with uniform initial moisture content, and saturated "piston" infiltration. Even with these non-realistic assumptions, if effectively parameterized, this method still generates useful and reliable results compared with other numerical and approximated approaches (Skaggs et al., 1969; Mein and Larson, 1973). Considering its advantages, Bouwer (1969) highlighted the utility of this method when taking into account the computational trade-offs with RE solutions.

Extensions of the Green-Ampt model beyond its initial assumptions have enabled its application to other natural infiltration cases, such as non-uniform soil profiles (Bouwer, 1969; Beven, 1984), and multistorm infiltration and redistribution (Ogden and Saghafian, 1997; Smith et al. 2002; Gowdish and Muñoz-Carpena, 2009). A particularly important case where an extension of the original assumption of the Green-Ampt model is necessary is when there is a WT. In general, depth-averaged soil moisture values in traditional infiltration equations like Green-Ampt (*i.e.* semi-infinite, uniform initial soil moisture) overpredict infiltration estimations when the soil is bounded by a WT. This is due to the difficulty in obtaining an equivalent initial uniform soil water content that effectively represents the real non-uniform water content condition with WT (Salvucci and Entekhabi, 1995; Chu, 1997). Recently, Liu et al. (2011) presented a modification to Craig et al. (2010)'s non-dimensional form of the Green-Ampt model to account for the presence of a WT. Although this modification is shown to provide acceptable results as compared with a RE solution for a range of WT depths, the method assumes an initial uniform soil water content profile, and its performance relies on an empirical correction between RE and standard Green-Ampt results. Alternatively, previous works (Childs, 1960; Holmes and Colville, 1970; Duke, 1972) have suggested describing the soil-water redistribution over a WT as an equilibrium hydrostatic condition (Fig. 1). This approach assumes a linear relationship of soil matric potential (h, [L]) and soil depth (z, [L], positive downwards from the surface), whereby the non-uniform water content of the soil (θ

99 [L^3L^{-3}]) is described by the soil water characteristic curve, $\theta = \theta(h)$ (Jury et al., 1991),

100 $$h = L - z \Rightarrow \theta = \theta(L - z) \quad (1)$$

101 where L [L] is the depth of the fixed shallow water table below the soil surface (i.e. the distance from the surface).
102 Based on this initial and boundary hydrostatic equilibrium conditions, Chu (1997) proposed an incremental calculation
103 technique to evaluate infiltration into ponded soils with a WT. This calculation relies on Bouwer's (1969) expression
104 of the Green-Ampt equation that accounts for infiltration of water into a non-uniform soil as,

105 $$t = \int_0^{z_F} \frac{1}{f}[\theta_s - \theta(L - z)]dz \quad (2)$$

106 where t [T] is time since the beginning of the event; θ_s [L^3L^{-3}] is the saturation water content; f [LT^{-1}] is the rate of
107 surface infiltration; z_F [L] is the wetting front depth. Following Neuman (1976) and Chu (1997), after substitution of
108 the equilibrium condition (eq. 1), the cumulative (F, [L]) and instantaneous infiltration (f, [LT^{-1}]) can be calculated by,

109 $$F = F_p = \int_0^{z_F}[\theta_s - \theta(L - z)]dz = \theta_s z_F + \int_L^{L-z_F} \theta(h)dh = \theta_s z_F - \int_{L-z_F}^{L} \theta(h)dh \quad (3)$$

110 $$f = f_p = K_s + \frac{1}{z_F}\int_0^{L-z_F} K(h)\mathrm{dh} = K_s - \frac{1}{z_F}\int_L^{z_F} K(L - z)\mathrm{dz} \quad (4)$$

111 where the subscript p denotes under ponding or "capacity", *i.e.* when the flux at the surface is not limited by available
112 water and is therefore maximum for each time; K_s and $K(h)$ [LT^{-1}] represents the soil saturated and unsaturated
113 hydraulic conductivity function, respectively. Chu (1997) proposed the solution to eq. (2-4) using sufficiently small
114 increments of z, $\Delta z = z_i - z_{i-1}$. If an initial value of F_1 and f_1 for the first Δz (from the surface to a small depth) is known,
115 then successive values of time ($t_i = t_{i-1} + \Delta t$) for each Δz can be approximated by substituting eq. (3) into (2) as,

116 $$t_i = t_{i-1} + \mathrm{dt} = t_{i-1} + \frac{F_i - F_{i-1}}{0.5(f_i + f_{i-1})} \quad (5)$$

117 Chu (1997) further proposed that a valid initial step could be obtained by assuming standard Green-Ampt conditions
118 (i.e. piston flow) from the surface, hydrostatic equilibrium of the surface water content with the WT (θ_o), and
119 calculating the suction at the wetting front (S_{av}) as (Bouwer, 1964),

120 $$S_{\mathrm{av}} = \frac{1}{K_s}\int_0^L K(h)\mathrm{dh} \quad (6)$$

121 Vachaud et al. (1974) was able to use experimental data to test the solution of this equation successfully. However,
122 their experimental data did not allow enough time to determine how the model would respond when the wetting front
123 reaches L.

124 An elegant and useful approximate solution to ponded infiltration with WT was proposed by Salvucci and Entekhabi
125 (1995). Their solution is based on the assumptions of initial hydrostatic equilibrium and uses Philip (1957) integral
126 approximation of RE (Fig. 1). This approximate solution is advantageous, as it describes not only the infiltration but

127 also soil water redistribution during infiltration, and the characteristics of the wetting front as it moves towards the WT
128 during long events. In addition, the method assumes a more realistic piecewise linear wetting front with a variable
129 slope during infiltration (α in Fig. 1). This algorithm was successful when compared with RE solution for three different
130 soil types and when tested with the soil moisture profile data from Vachaud and Thony (1971)'s experiments. However,
131 the applicability of the algorithm for coupling with commonly used hydrological models is limited as it requires ponded
132 conditions, Brooks and Corey's soil water function (Appendix, eq. A1), and similarly to the original Green-Ampt it
133 requires an implicit solution.

134 The overall objective of this work and its companion paper (Lauvernet and Muñoz-Carpena, 2017) is to analyse the
135 impact of the presence of a WT on VFS efficiency. In this first paper, we will expand the Green-Ampt-based infiltration
136 solution to soils bounded by WT under variable rainfall with no initial ponding. We accomplish this by combining
137 Salvucci and Entekhabi (1995) and Chu (1997) approaches with a generic solution technique, and developing novel
138 integral formulae to calculate the singular times (time to ponding, t_p, shift time t_0, and time to column saturation, t_w)
139 for soils with no initial ponding. We assess the ability of the simplified method to accurately predict surface infiltration
140 and water content predictions for a variety of soils as compared with RE numerical solutions and previously published
141 experimental data. An illustrative example of calculation during an unsteady rainfall event is also presented along with
142 examples of applications of the proposed algorithm to analyse the effects of WT depth. In the companion paper, we
143 couple the new shallow water infiltration algorithm with an existing VFS numerical model (VFSMOD, Muñoz-
144 Carpena et al., 1999; 2010; 2015) and analyse the effects on runoff, sediment and pesticide removal efficiency.

145 **2 Proposed algorithm**

146 **2.1 Infiltration rate in soils bounded by a WT with a non-ponded initial state and subject to constant rainfall**

147 In general, the infiltration rate (f[LT^{-1}]) of a WT bounded soil with uniform rainfall rate (i [LT^{-1}]) and no initial surface
148 ponding will have a similar profile to the example shown in Fig. 2a, described by,

149
$$\begin{cases} f = i & 0 < t \le t_p \\ f = f_p & t_p < t < t_w \\ f = \min(f_w, i) & t \ge t_w \end{cases} \quad (7)$$

150 The identification of three singular times during the infiltration calculations is necessary for a solution to eq. (7). These
151 singular times are: time to reach ponding (t_p) (which depends on the shift time, t_0 described later), and time to column
152 saturation (t_w), when the wetting front approaches the capillary fringe at depth z_w (see Fig. 1). The effective saturation
153 depth z_w relies on L and soil air entry pressure (h_b), z_w=L−h_b ($z_w \ge 0$; z_w=0 when L < h_b , i.e. the soil is effectively
154 saturated by the capillary fringe). Often, h_b is set at 0 (*i.e.* z_w=L), even if some of the soil characteristic functions take
155 the air entry pressure into account (Brooks and Corey, 1964; Clapp and Hornberger, 1978). At t_w, the soil column is
156 saturated and the rate of infiltration sharply drops to f_w, or i if i< f_w (Fig. 2a). t_w depends on L and the slope of *K(h)*
157 (Salvucci and Entekhabi, 1995). If the WT is very shallow, the time to saturation t_w can occur before the time to

ponding. Salvucci and Enthekabi, (1995) and Liu et al., (2011) initially proposed that the infiltration rate is equal to $f_w = K_s$, when $t \geq t_w$, meaning that the vertical hydraulic gradient at the initial WT is 1. However, in most field situations when the wetting front has reached the WT, the profile's hydraulic gradient is less than 1 and the proposed solution might overestimate the final infiltration rate. Instead, another solution is to consider that for $t \geq t_w$ the infiltration flow at the surface (Q_f) is controlled by lateral drainage flow (Q_L) at the downslope boundary of the simulated soil elementary volume (Fig. 1b), applicable to floodplain conditions typical of VFS. If we consider that the soil profile is saturated at $t \geq t_w$, with an effective saturation depth $z_w = L - h_b$, following Dupuit-Forchheimer assumptions (Van Hoorn and Van Der Molen, 1973) the discharge ($Q_f = Q_L$) can be estimated as,

$$\left.\begin{array}{l} Q_f = f_w w b \\ Q_L = K_{\mathrm{sh}} S w z_w \end{array}\right\} Q_f = Q_L \Rightarrow f_w \approx \frac{K_{sh} S_o z_w}{b} \tag{8}$$

where K_{sh} is the lateral (horizontal) soil saturated hydraulic conductivity, w and b are the width (VFS dimension perpendicular to the flow) and length (VFS dimension in the flow direction) of the VFS surface area, and S is the slope of the initial WT. In hillslope hydrological modelling S is typically assumed to equal soil surface slope (S_o) (Beven and Kirkby, 1979 ; Vertessy et al., 1993). If the position of the infiltration elementary volume is close to a draining stream where $S > S_o$, eq. (8) may underestimate the infiltration rate and a 2-dimensional drainage approach like Hooghoudt (1940) equation should be used instead (Kao et al., 2001; Ritzema, 1994; van Schilfgaarde, 1957). In the algorithm developed here, the two options for the boundary condition are implemented: with "lateral drainage" (eq. 8) and Vachaud's "vertical drainage" ($f_w = K_s$). In some field conditions, a mixture of both end time boundary conditions might be expected, requiring empirical weighing of the two conditions.

2.2. Calculation of singular time points

Following Mein and Larson (1973), time to ponding t_p is the time for $f_p = i$ (intersection of the curves in Fig. 2a), typically when the surface water content is equal to saturation (Fig. 2c). At $t = t_p$ the equivalent wetting front depth (z_p) can be calculated by equating eq. (4) and (7),

$$\left.\begin{array}{l} f_p = i \\ f_p = K_s - \frac{1}{z_p}\int_L^{z_p} K(L-z)\mathrm{d}z \end{array}\right| \Rightarrow z_p = \frac{-1}{i - K_s}\int_L^{z_p} K(L-z)\mathrm{d}z \tag{9}$$

Since equation (9) is implicit in $z_p \geq 0$, it can be solved for each time step by defining the function G_p: $\mathbb{R} \rightarrow \mathbb{R}$ and its derivative G'_p so that the root $z_p \in [0, z_w]$ (*i.e.* $G_p(z_p) = 0$) is the wetting front depth at t_p,

$$\begin{array}{l} G_p(z_p) = z_p + \frac{1}{i - K_s}\int_L^{z_p} K(L-z)dz \\ G'_p(z_p) = 1 + \frac{1}{i - K_s} K(L - z_p) \end{array} \tag{10}$$

where z_p can be obtained applying a bracketed Newton-Raphson algorithm (Press et al., 1992) obtaining,

$$z_p^{k+1} = z_p^k - \frac{G_p(z_p^k)}{G_p'(z_p^k)} \quad \text{with} \quad |z_p^{k+1} - z_p^k| < \varepsilon \tag{11}$$

where k is the Newton-Raphson iteration level, and ε the error tolerance (here ε =10^{-8}). From eq. (3) at $t=t_p$ and $z=z_p$, and $F_p= i \cdot t_p$ we obtain,

$$t_p = \frac{1}{i}(\theta_s z_p - \int_0^{z_p} \theta(L-z)dz) \tag{12}$$

Next to ensure that F_p (Eq. 3) and $F=i \cdot t_p$ match at the intersection of the two curves on $t=t_p$ (Fig. 2b), an abscissa translation (shift time, t_o) is applied to F_p (Mein and Larson, 1973). Setting $z=z_p$ on eq. (2) and (3) yields t_0 as,

$$t_0 = \int_0^{z_p} \frac{1}{f_p}[\theta_s - \theta(L-z)]\, dz \tag{13}$$

Lastly, t_w is determined by calculating the integral eq. (2) at $z_F = z_w = L - h_b$ (Fig. 1) and adjusting for t_p and t_o,

$$t_w = t_p - t_0 + \int_0^{z_w} \frac{1}{f_p}[\theta_s - \theta(L-z)]dz \tag{14}$$

and using eq. (3), the cumulative infiltration at t_w is determined by,

$$F_w = \theta_s z_w - \int_{h_b}^{L} \theta(h)dh \tag{15}$$

t_w is equivalent to the non-dimensional time X_c proposed by Liu et al., (2011) that relies on the empirical error correction between RE solution and the Green-Ampt model. However, here t_w (eq. (14)) is calculated analytically for the more general case of non-uniform soil water content.

2.3 Infiltration capacity algorithm after surface ponding

The solution of Salvucci and Entekhabi (1995) can be simplified by setting the wetting front slope to zero (*i.e.* a horizontal front (α=0) at the depth z_F, Fig.1). This approach reduces the solution, making it analogous to eq. (2), which was employed by Bouwer (1969) in his explanation of the Green-Ampt model's applicability. For initial non-ponding conditions, the equation becomes,

$$t = t_p - t_0 + \int_0^{z_F} \frac{\theta_s - \theta(L-z)}{K_s - \frac{1}{z_F}\int_L^{z_F} K(L-z)\mathrm{dz}}\mathrm{dz} \quad ; t_p < t < t_w \tag{16}$$

As the wetting front travels deeper into the soil, α could increase, contingent on the type of soil (e.g. α is larger for fine soils). However, as the wetting front approaches WT, the pore space available for infiltration is small, which limits the error of the calculations (Salvucci and Entekhabi, 1995). This assumption is tested in section 2.4.

For a given time t, to solve for z_F we specify the implicit function of eq. (16) G: $\mathbb{R} \rightarrow \mathbb{R}$ and its derivative G', so that the root $z_F \in [z_{i-1}, z_w]$ of the function G is equal to the new depth of the wetting front,

$$G(z_F) = t - t_p + t_0 - \int_0^{z_F} \frac{\theta_S - \theta(L-z)}{K_S - \frac{1}{z_F}\int_L^{z_F} K(L-z)\mathrm{d}z}\,dz \qquad G'(z_F) = -\frac{\theta_S - \theta(L-z)}{K_S - \frac{1}{z_F}\int_L^{z_F} K(L-z)\mathrm{d}z} \Bigg| \quad {z_F}^{k+1} = {z_F}^{k} - \frac{G({z_F}^{k})}{G'({z_F}^{k})} \quad \text{with} \quad |{z_F}^{k+1} - {z_F}^{k}| < \varepsilon \tag{17}$$

In summary, for each time increment the proposed algorithm computes the depth of the wetting front (eq. 17), F (eq. 3, 15) and f (eq. 4, 7 and 8) using the singular times auxiliary eq. (12-14). A bracketing step in the Newton-Raphson algorithm is necessary, as the function G is undefined outside its physical range ($z_p<z_F<z_w$) (Press et al., 1992). The proposed algorithm is generic in that it can be used with any soil hydraulic functions like those of Gardner (1958), van Genuchten (1980) or Brooks and Corey (1964) (Appendix A) if numerical integration is used. Here, we used a Gauss-Quadrature integration scheme (Abramowitz and Stegun, 1972; Press et al., 1992).

2.4 Infiltration of soils with a WT and variable rainfall without initial ponding

For real VFS field situations, unsteady rainfall without initial soil ponding must be considered. Non-uniform rainfall is described by a hyetograph as a series of constant rainfall periods j (*i.e.* $i=i_j$ for $t_j<t<t_{j+1}$). The runoff produced by excess infiltration (*i.e.* Hortonian) and WT saturation (*i.e.* Dunne) are then determined at each time by water balance at the surface without accounting for evaporation during the rain event (Chu, 1997),

$$\Delta P = \Delta F + \Delta s + \Delta \mathrm{RO} \Rightarrow \Delta P - \Delta F = \Delta s + \Delta \mathrm{RO} \tag{18}$$

where Δ is the increment for that rainfall period, P and RO [L] are cumulative precipitation and runoff (excess rainfall), respectively, and when present s is the surface storage ($0<s<s_{max}$) that acts as a reservoir that must be filled ($s=s_{max}$) before runoff is generated (Chu 1978; Skaggs and Khaleel, 1982). For each period, if there is excess at the surface ($\Delta P-\Delta F>0$), the excess is first distributed to to fill up the surface storage ($\Delta s \leq s_{max} - s$) and the remainder (if any) to runoff ($\Delta RO = \Delta P - \Delta F - \Delta s \geq 0$).

For non-ponding conditions at the beginning of the event t_p and t_0 must be calculated (eq. 12-14), otherwise if initial ponding is present $t_p= t_0=0$. If during a rainfall period the surface storage becomes zero, and if new i_{j+1} of the following period is larger than the infiltration rate at the end of the last period, t_p (and t_0) must be recomputed (eq. 12-14) for the subsequent rainfall event (Chu, 1978; Skaggs and Khaleel, 1982). Also, each time t_p, and t_0 are calculated, t_w has to be re-calculated.

To allow for predictions of soil water content redistribution during the event (Fig. 1) and to maintain mass balance during infiltration for alternating periods of ponding and non-ponding conditions, it is necessary to track the "effective" position of the wetting front z_F for periods with no ponding. To do this, the value of z_F must satisfy the total cumulative infiltration amount at every time step (Fig. 1) and F (eq. 3) becomes implicit in z_F. As before, the root $z_F \in [z_{F_{i-1}}, z_w]$ ($z_{F_{i-1}}$ is the wetting front depth at the previous time step) of the function G_F: $\mathbb{R} \rightarrow \mathbb{R}$ and its derivative such as:

$$\left.\begin{array}{c} G_F(z_F) = F - \int_0^{z_F}[\theta_s - \theta(L-z)]dz \\ G_F{}'(z_F) = -\theta_s + \theta(L - z_F) \end{array}\right| \Rightarrow \left|\begin{array}{c} z_F^{k+1} = z_F^k - \frac{G_F(z_F^k)}{G_F{}'(z_F^k)} \\ |z_F^{k+1} - z_F^k|\varepsilon \end{array}\right. \quad (19)$$

The wetting front depth estimates provided by the algorithm are key in many hydrological applications where the aim is to simulate the potential for direct contamination of the WT by pollutants.

The next section provides an illustrative application of the full algorithm (herein refereed as SWINGO: Shallow Water table INfiltration alGOrithm) under unsteady rainfall conditions, typical in VFS settings (see Supp. Materials for coding details, source code, inputs and outputs).

3 Testing and applications

3.1 Numerical testing

A first step to validate SWINGO is done for the case of initially ponded soil and steady rainfall by a comparison with a finite difference mass-conservative numerical solution of RE (Celia et al., 1990) using Nofziger and Wu, (2003)'s CHEMFLO-2000 model. We used four soils that represented a variety of attributes. The Brooks and Corey soil water attributes and hydraulic conductivity curves (Table 1) were used for the initial soil description, and this description was later compared with van Genuchten parameters yielding similar results (results not shown). The first 3 soils represent typical clay, silty loam, and sandy loam soils with a 1.50 m deep WT (Salvucci and Entekhabi, 1995). The fourth soil corresponds to a fine sandy soil experimentally studied by Vachaud and Thony (1971) with a WT at 1.01m.

The soil water initial condition in CHEMFLO-2000 was set to hydrostatic equilibrium with a WT (eq. 1). The bottom boundary condition was set to a fixed matric potential $h(z=L) = 0$, to be representative of a WT at depth L. To simulate rainfall, the top boundary condition is set to a mixed type boundary with the flux density equal to the specified rainfall rate and the critical matric potential equalling zero (Nofziger and Wu, 2003). To allow for the development of distinct t_p and t_w values during the simulation, the constant rates of rainfall were chosen based on the soil texture. This selection was done utilizing a ratio of i/K_s=6 for the fine soils (clay and silty loam) and i/K_s=2 for the coarse soils, corresponding to the sandy loam and fine sandy soils studied by Vachaud and Thony (1971).

The comparison of the relative infiltration rates (f/K_s) calculated by RE (symbols) and the proposed SWINGO (lines) for the case of vertical drainage end boundary condition ($f_w = K_s$) is shown in Figure 3. The performance of the algorithm is similar to RE for all soils studied. The median efficiency coefficients C_{eff} (Nash and Sutcliffe, 1970) ranged from 0.927–0.9997, with the highest values being for clay, and yielding statistically acceptable models at 0.01 level of significance (Ritter and Muñoz-Carpena, 2013) (Table 1). For the same clay soil with ponded conditions and a WT, Salvucci and Entekhabi (1995) reported errors of approximately 5% at time t_w, at the point when the wetting front reaches the WT saturation (z_w), and the infiltration rate switches to the saturated hydraulic conductivity $f_w=K_s$ (f/K_s =1). Smaller differences (1% for clay and sandy loam and 3% for the rest) were found between both solutions in our tests. These observations indicate that the simplification (horizontal wetting front, α=0) did not affect the predictive

ability of the rate infiltration. A crucial pattern to notice is that the estimates of time to ponding acquired across our tested soil types and normalized rates of rainfall closely matched the outputs of the RE solution. Our results also indicate that the use of the non-uniform integral equations (eq 9-12) effectively limit errors in the t_p estimation that sometimes occur when utilizing the Green-Ampt model (Barry et al., 1996).

Figure 4 displays the cumulative infiltration and the depth of the wetting front determined using eq (20-21) for the vertical drainage boundary condition for the cases from Table 1. Similar to the infiltration curves, z_F values exhibited a plateau at t_w as they reach column saturation (Fig. 4b), corresponding to the capillary fringe at a depth of $z_F = z_w = L - h_b$ (Fig. 1), and therefore are not equal to the depth of the WT (fine sand: L=1.01 m; other soil types: L=1.50 m).

As the simplified approach is able to produce reliable z_F predictions, it also allows for the depiction of the redistribution of the soil water content during infiltration. We display the predictions of soil water (Figure 5) calculated by the proposed algorithm (dashed lines) as compared with the outputs of the RE solution (solid lines) for the non-ponding numerical test examples used previously. The simplified model is able to identify the midpoint of the wetting front depth at all time points. Additionally, our simplification of including the horizontal wetting front (α=0) generates an accurate prediction of soil water at earlier time points for all soil types, but this prediction decays somewhat at later time points when approaching column saturation for fine soils. The model does not degrade at later time points for the sandy soil type when it matches a horizontal wetting front redistribution. As mentioned previously, because of the smaller pore space near column saturation, the mass errors generated by non-zero slopes stay negligible. The infiltration mass balance error at the end of the simulation (Fig. 4a) ranges from 3–8%. This range of error values is deemed satisfactory, as these errors are the summation of approximation errors of both the infiltration and redistribution of soil moisture generated during the simulation.

A quick comparison of execution times between CHEMFLO and SWINGO for the cases in Fig. 5 yielded small reduction of 1-5 s with SWINGO (CPU: 1.6 GHz Intel Core 2 Duo). These results are machine, computer and compiler dependent, where CHEMFLO finite differences solution is implemented in Java computer language (run in Oracle ® jre-8u144) and contains a graphical user interface not intended for optimized simulations. SWINGO was implemented as a command line application in Fortran (Intel ® Fortran Compiler v17.0.4). Admittedly, the differences will likely be smaller with optimized code and new developments of Richards equation implementations (e.g. de Maet et al., 2014). However, these small differences will likely be compounded in the context of throughput simulations where the algorithm will be used in some applications. For example, the model coupled in the companion paper (VFSMOD) is used in current long-term pesticide regulatory assessments (30 yr. daily time steps in the USA or 10 yr. daily time steps in EU) (Muñoz-Carpena et al., 2010; 2015). Considering ~1/3 to ~2/3 of days with rainfall-runoff, the model would be run between ~3000 and ~7000 times for a typical 30 yr. assessment. Under these this type of throughput applications conditions, even a marginal time improvement can prove advantageous. In addition to marginal speed benefits, the proposed algorithm is robust (from the direct integral solution) and has physical consistency with VFSMOD that uses the extension of Green-Ampt for unsteady rainfall conditions (Chu 1978 and Skaggs and Khaleel, 1982) without the presence of a shallow water table.

3.2 Experimental testing

The physics of the model were tested in a second step using experimental data from Vachaud et al. (1974) and Chu, (1997). The data collected in the laboratory represents infiltration under ponded conditions in a vertical column of fine sand soil with a WT at 0.925 m depth. To demonstrate the generality of the proposed algorithm, the Vachaud et al. (1974) measured soil hydraulic characteristics were fitted to van Genuchten soil water characteristic and related unsaturated hydraulic conductivity function based on Mualem (1976) simplification (vG:vG), and the later was also fitted to Gardner function (vG:Grd) (see Appendix A and soil parameters in Table 1). The goodness-of-fit of these hydraulic functions (inset of Fig. 6) shows a small improvement of the $K(h)$ function for Gardner over that of van Genuchten-Mualem against the experimental data.

The simulated relative infiltration rates obtained with the proposed algorithm matched the observed data well (C_{eff}= 0.913-0.942, RMSE for f= 5.07x10^{-6}-6.20x10^{-6}m/s), yielding statistically acceptable models at α=1% for vG:Grd and α=5% for vG:vG combinations (Ritter and Muñoz-Carpena, 2013) (Table 1). The main differences observed between approximated solutions with vG:Grd or vG:Grd soil water functions are near the time when the wetting front depth approaches the WT, with a small advance (~0.02 h) introduced by the vG:Grd option. These small differences are related to the slope of the wetting front being different than 0, especially close to the intersection with the WT at the end of the event (Fig. 5). Note also that in this experimental case no observed data was available for comparison at the time when the wetting front reached the WT.

In all, these results provide not only a test of the simplified model against experimental data, but also illustrate its robustness and flexibility to handle other soil hydraulic functions.

3.3 Illustration for unsteady rainfall conditions

The use of SWINGO to simulate realistic unsteady rainfall conditions is presented for a storm composed of 4 rainfall periods: i_1= 1 cm/h (0 < t ≤ 2.8 h), i_2=0.25 cm/h (2.8< t ≤ 4.2h), i_3= 1 cm/h (4.2 < t ≤ 5h) and i_4= 0.25 cm (5 < t ≤ 6.9 h) (Table 2 and Fig. 7). The soil is clay (Table 1) with bottom vertical drainage boundary condition and s_{max}=0 (*i.e.* no surface storage). At the beginning of the event the soil is not ponded and is in equilibrium with the WT at L=150 cm below the surface, so max(z_F) = z_w= L - h_b = 0.6 m (Fig. 7). For the initial period, we calculate first the time to ponding with eq. (9-12, 19) (t_p=4657.2 s=1.29 h), the corresponding t_0 (2319 s=0.64 h) with eq. (13), and the time to reach the WT t_w (16100 s=4.47 h) with eq. (14). Since the t_w is higher than the rainfall period and t_p lower than the rainfall period, infiltration is equal to the rainfall rate (f=i_1; 0<t<t_{p1}) before ponding. After ponding it follows the infiltration capacity curve described by the solution of eq (16-17). At the beginning of the second rain period, since the new rainfall rate is less than the infiltration rate at the end of the previous period (i_2=0.25 cm/h < f_p=0.52 cm/h) and t_w is still beyond the period, the infiltration rate equals the new rainfall rate (f=i_2). At the beginning of the third period, the new rainfall rate is larger than the corresponding potential infiltration rate at that time (i_3=1 cm/h > f_p=0.44 cm/h) and ponding starts again immediately such that the new t_p=t_3 (15000 s=4.2 h, beginning of the new rainfall period), and t_0 (13764 s=3.82 h) and t_w (18500 s= 5.14 h) are recalculated. Since t_w is beyond the period, the infiltration is maintained at capacity for

the duration of this rainfall period. For the last period, the rainfall rate is lower than the ending infiltration capacity for last period (i_4=0.25 cm/h <f_p =0.34 cm/h), and infiltration is initially set to the rainfall rate. However, since t_w is within this period, the soil saturates when the water front reaches the WT depth ($t \geq t_w$), and this results in saturated vertical drainage flow with unit hydraulic gradient f=f_w=K_s (eq. 7-8) until the end of the storm. The values of the wetting front position (z_F) in Table 2 are calculated from the solution of eq (17) during infiltration capacity (ponding) periods, and the equivalent depths described by eq. (21) during non-ponding periods. Similarly, cumulative totals are calculated with eq. (3) or (20), and excess rainfall amounts are calculated with the surface mass balance eq. (18) for every time step.

3.4 Evaluation of WT effects on infiltration under conditions of ponding and non-ponding

Figure 8 presents the effect of the WT depth variation (L=0-200 cm) and event duration (0.5 < D < 6.0 h) on cumulative infiltration under ponding conditions for the soils in Table 1. The two end time boundary conditions are compared: f_w vertical (a-d) and f_w lateral (e-h) with S_o = 0.02, b = 1 m and K_{sh} = K_s (eq. 8 and Table 1). For the conditions tested it is possible to identify three clearly defined regions (denoted I, II and III in Fig. 8) based on the influence of the WT depth on the cumulative infiltration. Region I (left, shaded in Fig. 8) represents the WT near the surface, *i.e.* when it is within the capillary fringe area L<h_b (Fig, 1). The position of the WT in this region does not affect infiltration since the soil column is already saturated regardless of L with F=D·f_w. Next, Region II (clear background on Fig. 8a-d) is the most sensitive to variations of WT depth, located between L=h_b and a limit depth (L= 125-180 cm) where the variation of F is small (slope less than 0.2%). This limit depends on the shape of the soil water characteristic curve for each soil. Finally, Region III represents a region where surface infiltration can be considered effectively decoupled from the presence of the WT.

Next, the robustness and physical behaviour of the algorithm under non-ponded initial conditions was tested with different rainfall rates (i=0.1-20 cm/h), event durations (D=1-12 h) and WT depths (L=0-400 cm). Fig. 9a-d summarizes the results for D=6 hours and the vertical drainage boundary condition (f_w = K_s). Two main effects are identified. Firstly, as expected F is insensitive to changes in L for rainfall intensities lower than K_s, when f=i (no ponding) and F=D·K_s. Notice that this effect, although present, is not visible in the clay soil (Fig. 9b) since the K_s is below the first isoline. Secondly, for rainfall rates above K_s, the sensitivity to L varies by soil, depending on h_b and the time to ponding values for each rainfall rate (eq. 12). As in the ponding case, the soil column is saturated when $L \leq h_b$, and there is no sensitivity below this depth. In finer, less permeable soils (Fig. 9a-b) ponding happens earlier for the same rainfall rate i, resulting in an increased sensitivity to L with lower rainfall rates. For the lateral drainage boundary condition, results are similar for the finer soils (Fig. 9e-f), but much more sensitive to WT depth and rainfall rate values for more permeable soils (Fig. 9g-h).

Importantly, since excess rainfall runoff (RO) is complementary to F (eq. 18), these results also quantify the important influence that the combined effects of WT, soil type and rainfall intensity can have on surface runoff flow and transport processes in the VFS.

Summary and Conclusions

Limitations in current modelling approaches hamper the evaluation of the effects of WTs on soil infiltration and runoff in vegetative filter strips (VFS). A promising way to overcome these issues is by utilizing simplified yet realistic specialized algorithms in conjunction with available hydrological models to evaluate the impact of WTs in the environment. Previously, Salvucci and Entekhabi, (1995) and Chu, (1997) recommended the use of Green-Ampt implicit integral equations to examine infiltration into ponded soils with WT. We developed and assessed a simplified generic algorithm that is appropriate for coupling with available hydrological models, in particular the study of WT effects on VFS runoff pollution control performance. The proposed SWINGO algorithm is generic— it can utilize any configuration of soil hydraulic functions— and can be operated under non-ponded, ponded, and realistic variable rainfall conditions to determine runoff (excess rainfall), infiltration, and soil-water redistribution during the event.

SWINGO performed well (*Ceff* from 0.91 to 0.99) in comparison with the RE solution and using experimental data on 5 representative soils. The algorithm also was able to describe successfully the soil water redistribution during the simulated event. These useful and reliable predictions indicate that the proposed approach incorporating a horizontal slope of the wetting front is suitable for most real-world applications. Through an application of our proposed SWINGO algorithm, we showed the sensitivity of the infiltration and excess runoff to the depth of the WT, the length and intensity of the rainfall event, the soil texture and drainage bottom condition.

Some of the limitations of the proposed algorithm are the assumptions of a homogeneous soil profile and horizontal wetting front for fine soils. Future research is recommended to determine the general validity of the assumption of a hydrostatic equilibrium and the proposed computation of singular points during the infiltration episode. Additional experimental testing of the model should be conducted using data collected under various experimental and natural conditions (especially during events long enough for the wetting front to reach the WT). As in real soils, a mixture of both end time lateral and vertical boundary conditions might be expected, these field studies could also investigate site and event characteristics for which these boundary conditions might be dominant or in relative influence.

As SWINGO was accurate, fast, and robust when analysing a variety of conditions, it is appropriate to couple with currently available hydrological models to gauge the influence of the presence of WTs on other landscape processes beyond the simulation of filter strips. The proposed integral equation has broader relevance as a step forward in improving the science of hydrologic modelling in general in many other settings; e.q. to study shallow water table effects on surface runoff, infiltration, flooding, transport, ecological and land use processes.

The dynamic coupling with VFS overland flow and sediment and pesticide transport processes is developed in the companion paper (Lauvernet and Muñoz-Carpena, 2017). Global sensitivity and uncertainty analysis of the coupled model is conducted to identify important input factors and their interactions that will provide better understanding of the fundamental processes controlling VFS efficiency under WT conditions, and guide users to select effective parameters for practical applications.

Appendix A

The Brooks and Corey (1964) soil water characteristic ($\theta=\theta(h)$) and hydraulic conductivity ($K=K(h)$) functions are defined as,

$$\begin{matrix} S_e = \frac{\theta-\theta_r}{\theta_s-\theta_r} = & \begin{cases} (h/h_b)^{-\lambda} & ; h > h_b \\ 1 & ; h_b \geq h \end{cases} \\ K(h) = & K_s S_e{}^{\eta} \end{matrix} \quad \text{(A1)}$$

with h_b = bubbling pressure [L, < 0] ; λ =Brooks and Corey pore size index (shape parameter); η = Brooks & Corey hydraulic conductivity shape parameter, often η = 3+2/λ. θ_s and θ_r are the saturated and residual water content [L^3L^{-3}].

The van Genuchten (1980) soil water characteristic and hydraulic conductivity curves are defined as,

$$\begin{matrix} S_e = \frac{\theta-\theta_r}{\theta_s-\theta_r} = & \begin{cases} (1+(\alpha_{\mathrm{vG}}h)^n)^{-m} & ; h > 0 \\ 1 & ; h \leq 0 \end{cases} \\ K(h) = & K_s S_e{}^{1/2}(1-(1-S_e{}^{1/m})^m)^2 \end{matrix} \quad \text{(A2)}$$

where α_{vG} [L^{-1}] > 0, n, m are shape parameters. The Gardner (1958) unsaturated hydraulic conductivity function is given by,

$$K(h) = \begin{cases} \frac{K_s}{1+(h/h_c)^{n_{\mathrm{Grd}}}} = \frac{K_s}{1+(\alpha_{\mathrm{Grd}}h)^{n_{\mathrm{Grd}}}} & ; h > 0 \\ K_s & ; h \leq 0 \end{cases} \quad \text{(A3)}$$

where h_c=1/α_{Grd} = matric potential constant (5 < h_c < 50), and n_{Grd} = empirical constant (1.8 < n_{Grd} < 3.5).

Nomenclature

h	[L]	soil matric potential	h_b	[L]	capillary suction (bubbling pressure)
$\theta=\theta(h)$	[L^3L^{-3}]	soil water characteristic	θ_s	[L^3L^{-3}]	saturated water content
$K = K(h)$	[LT^{-1}]	hydraulic conductivity	K_s	[LT^{-1}]	saturated hydraulic conductivity
F	[L]	cumulative infiltration	F_p	[L]	cumulative infiltration at t_p
f	[LT^{-1}]	actual infiltration at surface	f_p	[LT^{-1}]	infiltration capacity (ponding)
i	[LT^{-1}]	rainfall rate	L	[L]	water table depth
S_{av}	[L]	suction at the wetting front	z_F	[L]	depth of the wetting front
t_w	[T]	time to column saturation	z_w	[L]	effective depth of saturation

t_p	[T]	time to ponding	z_p	[L]	wetting front depth at t_p
t_0	[T]	shift ponding time	RO	[L]	cumulative excess rainfall
P	[L]	cumulative precipitation	s	[L]	surface storage
D	[T]	storm duration			

418

419 **Author contribution**

420 RMC and CL developed conceptual model, code and testing. NC contributed to the theoretical development. RMC and
421 CL prepared the manuscript with contributions from all co-authors.

422 **Acknowledgements**

423 We thank G. Salvucci for providing valuable insight and relevant information from his original efforts on this topic,
424 J.V. Giráldez for providing useful and important references for this project, and J. Vanderborght for his invaluable
425 comments on the lateral drainage boundary condition development. We also thank the ECPA, DGPAAT and IRSTEA
426 for financial support during RMC's sabbatical in France that made this research possible. RMC also acknowledges the
427 UF Research Foundation Professorship, UF Water Institute Fellowship, and USDA NIFA Award No. 2016-67019-
428 26855 that provided additional support.

429 **References**

430 Abramowitz M., Stegun I.A.: Handbook of Mathematical Functions with Formulas, Graphs, and Mathematical Tables.
431 National Bureau of Standards Applied Mathematics Series 55. 10th Printing, 1972.

432 Abu-Zreig, M.: Factors affecting sediment trapping in vegetated filter strips: simulation study using VFSMOD.
433 Hydrological Processes 15, 1477–1488. doi:10.1002/hyp.220, 2001.

434 Arora, K., Mickelson, S.K., Helmers, M.J., Baker, J.L.: Review of Pesticide Retention Processes Occurring in Buffer
435 Strips Receiving Agricultural Runoff1. JAWRA Journal of the American Water Resources Association 46, 618–647,
436 doi:10.1111/j.1752-1688.2010.00438.x, 2010.

437 Barry, D. A., Parlange, J.-Y., Haverkamp, R.: Comment on "Variable-Head Ponded Infiltration Under Constant or
438 Variable Rainfall" by J. R. Philip, Water Resour. Res., 32(5), 1467–1469, doi:10.1029/95WR03645, 1996.

439 Basha HA.: Multidimensional linearized nonsteady infiltration toward a shallow water table. Water Resour. Res.,
440 36(9):2567-2573, doi:200010.1029/2000WR900150, 2000.

441 Beven K., J., Kirkby M.J.: A physically based variable contributing area model of basin hydrology. Hydrological
442 Sciences Bulletin, 24:43-69, doi: 10.1080/02626667909491834, 1979.

443 Beven K.: Infiltration into a class of vertically non-uniform soils. Hydrological Sciences Journal, 29(4), 425,
444 doi:10.1080/02626667909491834, 1984.

445 Beven, K. TOPMODEL: A critique. Hydrol. Proc., 11, 1069-1085, 1997.

446 Bouwer H.: Infiltration of water into nonuniform soil. J. Irrigat. Drain. Div., 95(IR4):451–462, 1969.

447 Bouwer H.: Unsaturated flow in ground-water hydraulics. Hydraul. Div. Amer. Soc. Civil Eng., 90(HY5), 121-144,
448 1964.

449 Brooks, RH, Corey AT.: Hydraulic properties of porous media. Hydrol. Paper., 3, 1964.

450 Carluer, N., Lauvernet, C., Noll, D., Muñoz-Carpena, R.: Defining context-specific scenarios to design vegetated
451 buffer zones that limit pesticide transfer via surface runoff, Sci. Total Env., 575, 701-712,
452 doi:10.1016/j.scitotenv.2016.09.105, 2017.

453 Celia M.A., Bouloutas E.T., Zarba RL.: A general mass-conservative numerical solution for the unsaturated flow
454 equation. Water Resour. Res., 26(7):1483-1496, 1990.

455 Childs E.C..: The nonsteady state of the water table in drained land. J. Geophys. Res., 65(2), 780-782, 1960.

456 Chu ST.: Infiltration during an unsteady rain. Water Resour. Res., 14(3), 461-466, 1978.

457 Chu ST.: Infiltration model for soil profiles with a water table. Trans. ASAE., 40(4), 1041-1046, 1997.

458 Clapp, R. B., and G. M. Hornberger: Empirical equations for some soil hydraulic properties, Water Resour. Res., 14(4),
459 PP. 601-604, 1978.

460 Craig JR, Liu G, Soulis ED.: Runoff–infiltration partitioning using an upscaled Green–Ampt solution. Hydrol.
461 Process.24, 2328-2334, doi:10.1002/hyp.7601, 2010.

462 Dosskey, M.G., Helmers, M.J., Eisenhauer, D.E.: A design aid for sizing filter strips using buffer area ratio. Journal of
463 Soil and Water Conservation 66, 29–39. doi:10.2489/jswc.66.1.29, 2011.

464 Dosskey, M.G., Helmers, M.J., Eisenhauer, D.E.: An Approach for Using Soil Surveys to Guide the Placement of Water
465 Quality Buffers. Journal of Soil and Water Conservation 61, 344–354, 2006.

466 Dosskey, M.G.: Toward quantifying water pollution abatement in response to installing buffers on crop land. Environ
467 Manage 28, 577–598, doi: 10.1007/s002670010245, 2001.

468 Duke HR. Capillary properties of soils - influence upon specific yield. Trans. ASAE. 15(4):688-691, 1972.

469 Fox, G., Muñoz-Carpena, R., Sabbagh, G.: Influence of flow concentration on parameter importance and prediction
470 uncertainty of pesticide trapping by vegetative filter strips. J. Hydrol., 384, 164-173,
471 doi:10.1016/j.jhydrol.2010.01.020, 2010.

472 Fox, G.A., Sabbagh, G.J.: Comment on "Major Factors Influencing the Efficacy of Vegetated Buffers on Sediment
473 Trapping: A Review and Analysis," by Xingmei Liu, Xuyang Zhang, and Minghua Zhang in the 2008 37:1667–1674.
474 Journal of Environmental Quality, 38, 1-3. doi:10.2134/jeq2009.0001le, 2009.

475 Gardner WR.: Some steady-state solutions of the unsaturated moisture flow equation with application to evaporation
476 from a water table. Soil Sci., 85(4):228-232, 1958.

477 Gillham, R.W.: The capillary fringe and its effect on water-table response, J. Hydrol., Volume 67, Issue 1, Pages 307-
478 324, ISSN 0022-1694, http://dx.doi.org/10.1016/0022-1694(84)90248-8, 1984.

479 Gowdish L, Muñoz-Carpena R: An improved Green-Ampt infiltration and redistribution method for uneven multistorm
480 series. Vadose Zone J., 8:470-479, doi: 10.2136/vzj2008.0049, 2009.

481 Green WH, Ampt GA.: Studies on Soil Physics, J. Agr.Sci., 4:1-24, 1911.

482 Haan CT, Barfield BJ, Hayes JC.: Design hydrology and sedimentology for small catchments. San Diego, Calif.:
483 Academic Press, 1994.

484 Holmes JW, Colville JS.: Forest hydrology in a karstic region of Southern Australia. J. Hydrol., 10(1):59-74, 1970.

485 Hooghoudt, S.B.: Algemene beschouwing van het probleem van de detailontwatering en de infiltratie door middel van
486 parallel loopende drains, greppels, slooten en kanalen. No. 7 in de serie: Bijdragen tot de kennis van eenige
487 natuurkundige grootheden van den grond. Bodemkundig Instituut te Groningen. Rijksuitgeverij Dienst van de
488 Nderlandse Staatscourant. 's-Gravenhage, Algemeene Landsdrukkerij, 1940.

489 Jury WA, Gardner WR, Gardner WH.: Soil Physics, 5th Edition. John Wiley & Sons, New York, 1991.

490 Kao, C., Bouarfa, S., Zimmer, D.:. Steady state analysis of unsaturated flow above a shallow water-table aquifer
491 drained by ditches. J. Hydrol., 250, 122–133, doi: 10.1016/S0022-1694(01)00426-7, 2001.

492 Lacas, J.-G., Carluer, N., Voltz, M.: Efficiency of a Grass Buffer Strip for Limiting Diuron Losses from an Uphill
493 Vineyard Towards Surface and Subsurface Waters. Pedosphere, 22, 580–592, doi: 10.1016/S1002-0160(12)60043-5,
494 2012.

495 Lacas, J.-G., Voltz, M., Gouy, V., Carluer, N., Gril, J.-J.: Using grassed strips to limit pesticide transfer to surface water:
496 a review. Agron. Sustain. Dev. 25, 253–266, doi:10.1051/agro:2005001, 2005.

Lambrechts, T., François, S., Lutts, S., Muñoz-Carpena, R. and Bielders, C. L.: Impact of plant growth and morphology and of sediment concentration on sediment retention efficiency of vegetative filter strips: Flume experiments and VFSMOD modeling, J. Hydrol., 511, 800–810, doi:10.1016/j.jhydrol.2014.02.030, 2014.

Lauvernet, C. and Muñoz-Carpena, R.: Shallow water table effects on water, sediment and pesticide transport in vegetative filter strips: Part B. model coupling, application, factor importance and uncertainty, Hydrol. Earth Syst. Sci. Discuss. doi:10.5194/hess-2017-406, in review, July 2017.

Liu G, Craig JR, Soulis ED:Applicability of the Green-Ampt infiltration model with shallow boundary conditions. J. Hydrologic Eng., 16:266, doi:10.1061/(ASCE)HE.1943-5584.0000308, 2011.

de Maet T, Hanert, E and Vanclooster, M: A fully- explicit discontinuous Galerkin hydrodynamic model for variably-saturated porous media. Journal of Hydrodynamics 26(4):594-607, doi:10.1016/S1001-6058(14)60067-6, 2014.

Mein RG, Larson CL. Modeling infiltration during a steady rain. Water Resour. Res., 384–394, 1973.

Miller CT, Williams GA, Kelley CT, Tocci MD.: Robust solution of Richards'equation for non uniform porous media. Water Resour. Res., 34(10):2599–2610, doi:199810.1029/98WR01673, 1998.

Mualem Y. A new model for predicting the hydraulic conductivity of unsaturated porous media. Water Resour. Res., 12(3):513-522, doi:10.1016/j.cageo.2007.12.002, 1976.

Muñoz-Carpena, R. & Parsons, J. E.: A design procedure for vegetative filter strips using VFSMOD-W, Transactions of the ASAE 47(6), 1933—1941, doi :10.13031/2013.17806, 2004.

Muñoz-Carpena, R., Fox, G., Sabbagh, G.: Parameter Importance and Uncertainty in Predicting Runoff Pesticide Reduction with Filter Strips. Journal of Environmental Quality, 39, 630–641. doi:10.2134/jeq2009.0300, 2010.

Muñoz-Carpena, R., Parsons, J.E., Gilliam, J.W.: Modeling hydrology and sediment transport in vegetative filter strips. J. Hydrol,. 214, 111–129. doi:10.1016/S0022-1694(98)00272-8, 1999.

Muñoz-Carpena, R., Ritter, A., Fox G.A., Perez-Ovilla O.: Does mechanistic modeling of filter strip pesticide mass balance and degradation affect environmental exposure assessments? Chemosphere 139:410-421. doi:10.1016/j.chemosphere.2015.07.010, 2015.

Muscutt, A.D., Harris, G.L., Bailey, S.W., Davies, D.B.: Buffer zones to improve water quality: a review of their potential use in UK agriculture. Agriculture, Ecosystems & Environment, 45, 59–77, doi:10.1016/0167-8809(93)90059-X, 1993.

Nash JE, Sutcliffe JV.: River flow forecasting through conceptual models, part I - A discussion of principles. J. Hydrol., 10:282-290, 1970.

Neuman SP. Wetting front pressure head in the infiltration model of Green and Ampt. Water Resour. Res., 12(3):564-566, doi:197610.1029/WR012i003p00564, 1976.

Nofziger DL, Wu J.: CHEMFLO-2000: Interactive software for simulating water and chemical movement in unsaturated soils. U.S.EPA, Cincinnati, Ohio: Rep. EPA/600/R-03/008. National Risk Management Research Laboratory Office of Research and Development, 2003.

Ogden FL, Saghafian B. Green and Ampt infiltration with redistribution. J. Irrigat. Drain. Eng., 123, 5, 1997.

Ogden, FL, W. Lai, R.C. Steinke, and J. Zhu: Validation of finite water-content vadose zone dynamics method using column experiment with a moving water table and applied surface flux. Water Resour. Res., 51, doi:10.1002/2014WR016454, 2015.

Ohliger, R, Schulz, R: Water body and riparian buffer strip characteristics in a vineyard area to support aquatic pesticide exposure assessment. Sci. Total Env., 408(22):5405-13. DOI: 10.1016/j.scitotenv.2010.08.025, 2010.

Paniconi C, Putti M.: A comparison of Picard and Newton iteration in the numerical solution of multidimensional variably saturated flow problems. Water Resour. Res., 30(12), 3357, doi:10.1029/94WR02046, 1994.

Philip JR.: The theory of infiltration: 1. the infiltration equation and its solution. Soil Sci., 83, 5, 345-358, 1957.

Poletika, N.N., Coody, P.N., Fox, G.A., Sabbagh, G.J., Dolder, S.C., White, J.: Chlorpyrifos and Atrazine Removal from Runoff by Vegetated Filter Strips: Experiments and Predictive Modeling. Journal of Environmental Quality, 38, 1042–1052. doi:10.2134/jeq2008.0404, 2009.

Press WH, Flannery BP, Teukolsky SA, Vetterling, WT.: Numerical Recipes in Fortran 77: The Art of Scientific Computing. Cambridge University Press, 1992.

Rawls WJ, Brakensiek DL, Miller N.: Green-Ampt infiltration parameters from soils data. J. Hydraul. Eng., 109(1), 62-70, 1983.

Rawls WJ, Brakensiek DL, Saxton KE.: Estimation of soil water properties. Trans. ASABE., 25(5), 1316-1320, 1982.

Reichenberger S, Bach M, Skitschak A, Frede H-G.: Mitigation strategies to reduce pesticide inputs into ground- and surface water and their effectiveness: a review. Sci. Total Environ., 384, 1-35, doi:10.1016/j.scitotenv.2007.04.046, 2007.

Richards LA.: Capillary conduction of liquids through porous mediums. Physics., 1(5), 318, 1931.

Ritter, A., Muñoz-Carpena, R.: Performance evaluation of hydrological models: Statistical significance for reducing subjectivity in goodness-of-fit assessments. J. Hydrol. 480, 33–45, doi:10.1016/j.jhydrol.2012.12.004, 2013.

554 Ritzema, H.P.: Subsurface flow to drains. Chapter 8 in: H.P.Ritzema (ed.), Drainage Principles and Applications, Publ.
555 16, pp. 236-304, International Institute for Land Reclamation and Improvement (ILRI), Wageningen, The Netherlands.
556 ISBN 90 70754 3 39, 1994.

557 Ross PJ.: Modeling soil water and solute transport—fast, simplified numerical solutions. Agron. J., 95(6), 1352,
558 doi:10.2134/agronj2003.1352, 2003.

559 Sabbagh, G.J., Fox, G.A., Kamanzi, A., Roepke, B., Tang, J.-Z.: Effectiveness of Vegetative Filter Strips in Reducing
560 Pesticide Loading: Quantifying Pesticide Trapping Efficiency. J. Environ. Qual. 38, 762. doi:10.2134/jeq2008.0266,
561 2009.

562 Sabbagh, G.J., Muñoz-Carpena, R. and Fox, G.A. 2013. Distinct influence of filter strips on acute and chronic pesticide
563 aquatic environmental exposure assessments across U.S. EPA scenarios. Chemosphere 90(2):195-
564 202. doi:10.1016/j.chemosphere.2012.06.034

565 Salvucci GD, Entekhabi D.: Ponded infiltration into soils bounded by a water table. Water Resour. Res., 31, 2751-
566 2759, doi:10.1029/95WR01954, 1995.

567 Seibert J, Rodhe A, Bishop K.: Simulating interactions between saturated and unsaturated storage in a conceptual
568 runoff model. Hydrol. Process., 17(2), 379-390, doi:10.1002/hyp.1130, 2003.

569 Simpkins W, Wineland T, Andress R, Johnston D, Caron G, Isenhart T, Schultz R.: Hydrogeological constraints on
570 riparian buffers for reduction of diffuse pollution: examples from the Bear Creek watershed in Iowa, USA. Water
571 Science and Tech. 45, 61–68, 2002.

572 Singh VP, Woolhiser DA.: Mathematical Modeling of Watershed Hydrology. J. Hydrologic Eng., 7(4), 270-292,
573 doi:10.1061/(ASCE)1084-0699(2002)7:4(270), 2002.

574 Skaggs RW, Huggins LF, Monke EJ, Foster GR.: Experimental evaluation of infiltration equations. Trans. ASAE.,
575 12(6), 822-828, 1969.

576 Skaggs RW, Khaleel R.: Infiltration in hydrologic modeling of small watersheds. ASAE Mon. St. Joseph, MI: Am.
577 Soc. Agr. Engrs., 1982.

578 Smith RE, Corradini C, Melone F.: Modeling infiltration for multistorm runoff events. Water Resour. Res., 29(1), 133-
579 144, doi:199310.1029/92WR02093, 1993.

580 Smith RE, Smettem KRJ, Broadbridge P.: Infiltration theory for hydrologic applications. American Geophysical
581 Union, Washington, DC: Water Res. M., 15, 2002.

582 Srivastava R, Yeh T-CJ.: Analytical solutions for one-dimensional, transient infiltration toward the water table in
583 homogeneous and layered soils. Water Resour. Res., 27(5), 753-762, doi:199110.1029/90WR02772, 1991.

584 Talbot, C. A., and F. L. Ogden: A method for computing infiltration and redistribution in a discretized moisture content
585 domain, Water Resour. Res., 44, W08453, doi:10.1029/2008WR006815, 2008.

586 Vachaud G, Gaudet JP, and Kuraz V.: Air and water flow during ponded infiltration in a vertical bounded column of
587 soil. J. Hydrol., 22, 89-108, doi: 10.1016/0022-1694(74)90098-5, 1974.

588 Vachaud G, Thony JL.: Hysteresis during infiltration and redistribution in a soil column at different initial water
589 contents. Water Resour. Res., 7, 111-127, doi:197110.1029/WR007i001p00111, 1971.

590 van Genuchten MT.: A closed-form equation for predicting the hydraulic conductivity of unsaturated soils. Soil Sci.
591 Soc. Am. J., 44, 892-898, 1980.

592 van Hoorn J.W., van Der Molen W.H.: Drainage of sloping lands. Design and management of drainage systems, 329-
593 339, 1973.

594 van Schilfgaarde, J.: Approximate solutions to drainage flow problems. In: J.N. Luthin (Ed.), Drainage of agricultural
595 lands, p.79-112. Agron. Monogr. 7. ASA, Madison, WI, USA, 1957.

596 Vertessy R.A., Hatton T.J., O'Shaughnessy P.J., Jayasuriya M.D.A.: Predicting water yield from a mountain ash forest
597 catchment using a terrain analysis based cathment model, J. Hydrol., 665-700, doi:10.1016/0022-1694(93)90131-R,
598 1993.

599 Vogel T, van Genuchten MT, Cislerova M.: Effect of the shape of the soil hydraulic functions near saturation on
600 variably-saturated flow predictions. Adv. Water Resour., 24(2), 133-144, doi:10.1016/S0309-1708(00)00037-3, 2001.

601 Wu, L., Muñoz-Carpena, R., Gao, B., Yang, W. and Pachepsky, Y. A.: Colloid Filtration in Surface Dense Vegetation:
602 Experimental Results and Theoretical Predictions, Environ. Sci. Technol., 48(7), 3883–3890, doi:10.1021/es404603g,
603 2014.

604 Yu, C., Muñoz-Carpena, R., Gao, B. and Perez-Ovilla, O.: Effects of ionic strength, particle size, flow rate, and
605 vegetation type on colloid transport through a dense vegetation saturated soil system: Experiments and modeling, J.
606 Hydrol., 499, 316–323, doi:10.1016/j.jhydrol.2013.07.004, 2013.

Table 1. Parameters used in numerical and experimental testing of SWINGO. Nash and Sutcliffe coefficient of efficiency (C_{eff}) and root mean error (RMSE) represent SWINGO infiltration goodness-of-fit with Richards' finite differences solution (CHEMFLO-2000) and experimental data from Vachaud et al. (1974).

Numerical testing[†]

Soil	L (m)	θ_r	θ_s	K_s ($m \cdot s^{-1}$)	h_b (m)	λ	η	C_{eff}[†††,††††]	RMSE[†††] $f(x10^{-6}\ m \cdot s^{-1})$
Silty Loam	1.5	0	0.35	$3.40x10^{-6}$	0.450	1.20	4.67	0.994[0.969-0.999]***	0.309[0.119-0.541]
Clay	1.5	0	0.45	$3.40x10^{-7}$	0.900	0.44	7.54	0.999[0.998-1.000]***	0.015[0.003-0.028]
Sandy Loam	1.5	0	0.25	$3.40x10^{-5}$	0.250	3.30	3.61	0.985[0.882-0.998]***	1.326[0.578-2.414]
Vachaud and Thony (1971)	1.01	0	0.35	$1.75x10^{-5}$	0.181	0.73	4.63	0.927[0.821-0.977]***	1.488[0.893-2.240]

Experimental testing[†,††]

Soil Vachaud et al. (1974)	L (m)	θ_r	θ_r	K_s ($m.s^{-1}$)	α_{vG} (m^{-1})	n	m	α_{Grd} (m^{-1})	n_{Grd}	C_{eff}[†††,††††]	RMSE[†††] $f(x10^{-6}\ m \cdot s^{-1})$
vG:vG	0.925	0.107	0.34	$2.64x10^{-5}$	1.143	2.363	0.652	-	-	0.913[0.742-0.951]**	6.204[4.726-7.920]
vG:Grd	0.925	0.107	0.34	$2.64x10^{-5}$	1.143	2.363	0.652	0.136	2.151	0.942[0.828-0.971]***	5.069[3.696-6.468]

[†] h_b, λ, η are the Brooks and Corey parameters; [††] α_{vG}, n, and m are van Genuchten parameters, and α_{Grd} and n_{Grd} are the Gardner parameters (see Appendix for details); [†††] median value [95% confidence interval in brackets]; [††††] models were statistically acceptable at a significance level of 0.01 (***) or 0.05 (**) (Ritter and Muñoz-Carpena, 2013)

Table 2. Infiltration and excess runoff calculations for an illustrative unsteady rainfall event on a clay soil with no initial ponding at equilibrium with a shallow water table at 150 cm depth, s_{max}=0 and end vertical boundary condition. The + sign in the first column represents any time right after the time step.

Time, t (s)	t_p (s)	t_0 (s)	t_w (s)	i (m/s)	P (m)	f (m/s)	F (m)	RO (m)	z_F (m)
0	4657.2	2319.0	16100	$2.78\text{x}10^{-6}$	0	$2.78\text{x}10^{-6}$	0.0000	0	0
4657.2	4657.2	2319.0	16100	$2.78\text{x}10^{-6}$	0.0129	$2.78\text{x}10^{-6}$	0.0129	0	0.017
7500				$2.78\text{x}10^{-6}$	0.0208	$1.83\text{x}10^{-6}$	0.0192	0.0016	0.253
10000				$2.78\text{x}10^{-6}$	0.0278	$1.46\text{x}10^{-6}$	0.0233	0.0045	0.327
10000^{+}				$7.00\text{x}10^{-7}$	0.0278	$7.00\text{x}10^{-7}$	0.0233	0.0045	0.327
15000				$7.00\text{x}10^{-7}$	0.0313	$7.00\text{x}10^{-7}$	0.0268	0.0045	0.408
15000^{+}	15000	13763.7	18500	$2.78\text{x}10^{-6}$	0.0313	$1.21\text{x}10^{-6}$	0.0268	0.0045	0.408
16500	15000	13763.7	18500	$2.78\text{x}10^{-6}$	0.0354	$1.08\text{x}10^{-6}$	0.0285	0.0069	0.461
18000				$2.78\text{x}10^{-6}$	0.0396	$9.49\text{x}10^{-7}$	0.0300	0.0096	0.535
18000^{+}				$7.00\text{x}10^{-7}$	0.0396	$7.00\text{x}10^{-7}$	0.0300	0.0096	0.535
18500				$7.00\text{x}10^{-7}$	0.0399	$7.00\text{x}10^{-7}$	0.0304	0.0096	0.569
18500^{+}				$7.00\text{x}10^{-7}$	0.0399	$3.40\text{x}10^{-7}$	0.0304	0.0096	0.600
25000				$7.00\text{x}10^{-7}$	0.0445	$3.40\text{x}10^{-7}$	0.0326	0.0119	0.600
25000^{+}				0	0.0445	0	0.0326	0.0119	0.600

FIGURE CAPTIONS

Figure 1: Conceptual depiction of infiltration and soil water redistribution for soils with shallow water table for: a) time before wetting front reaches the water table; and b) time after the wetting front reaches the water table ($t \geq t_w$), where surface infiltration flow (Q_f) is limited by lateral Boussinesq subsurface flow (Q_L). See explanation of symbols in the text.

Figure 2: Conceptual curves of (a) infiltration rate, f; (b) cumulative infiltration, F; and (c) soil water redistribution, θ, under shallow water table, for soil without initial ponding, and constant rainfall rate (i) conditions. The singular times for ponding (t_p), shifting (t_0) and to reach column saturation (t_w), and final infiltration rate (f_w) after the wetting front reaches the water table ($t \geq t_w$) are represented.

Figure 3: Comparison of normalized infiltration rates (f/K_s) for soils without initial ponding described in Table 1, with vertical drainage (Vachaud) bottom boundary (f_w) condition. Lines represent the simplified model results. Symbols represents Richards equation numerical solution. The rainfall rate i was selected based on the saturated hydraulic conductivity (K_s) for each soil to ensure ponding at the surface.

Figure 4: Comparison of (a) cumulative infiltration (F) and (b) wetting front depth (z_F) movement results. Lines represent the simplified model and symbols represent Richards equation numerical solution for soils without initial ponding in Table 1 with vertical drainage (Vachaud) bottom boundary (f_w) condition.

Figure 5: Comparison of soil water (θ) redistribution between Richards equation numerical solution (solid lines) and the simplified model (dashed lines) during infiltration without initial ponding and with vertical drainage (Vachaud) bottom boundary condition (f_w) for soils in Table 1.

Figure 6: Comparison of the simplified and RE results against Vachaud et al. (1974) experimental data set (figure body), and fitting of soil water characteristics to different equations (inset). vG and Grd represent respectively the van Genuchten and Gardner's soil characteristic curves used to parametrize the simplified and RE models (see Table 1 for details).

Figure 7: Simulation of unsteady rainfall event on the clay soil in initial equilibrium with a shallow water table at 150 cm depth, non-ponded conditions and vertical drainage (Vachaud) bottom boundary condition (f_w): a) infiltration (f) and rainfall rates (i, subindices in i_1 to i_4 represent the rainfall periods within the hyetograph); b) cumulative rainfall (P), infiltration (F), excess runoff (RO) and wetting front depth (z_F) during the event.

Figure 8: Effect of water table depth (L) on cumulative infiltration (F, represented by isolines) for distinct soils under initial ponding and different durations of infiltration events (D) for four types of soils and two end drainage bottom boundary conditions (f_w): (a-d) vertical and (e-h) lateral (S_o= 0.02, b = 1 m, and here $K_{sh} = K_s$ from Table 1).

Figure 9: Change in cumulative infiltration (F) as a function of rainfall rate (i) and water table depth (L) under non-ponded initial conditions after a rainfall duration D=6 hour for the four types of soils in Table 1 and two end drainage bottom boundary conditions (f_w): (a-d) vertical and (e-h) lateral (S_o= 0.02, b = 1 m, and here $K_{sh} = K_s$ from Table 1). The isolines describe the change of F with water table depth for the same rainfall rate (i). h_b the bubbling pressure (capillary fringe) for each soil type (Table 1).

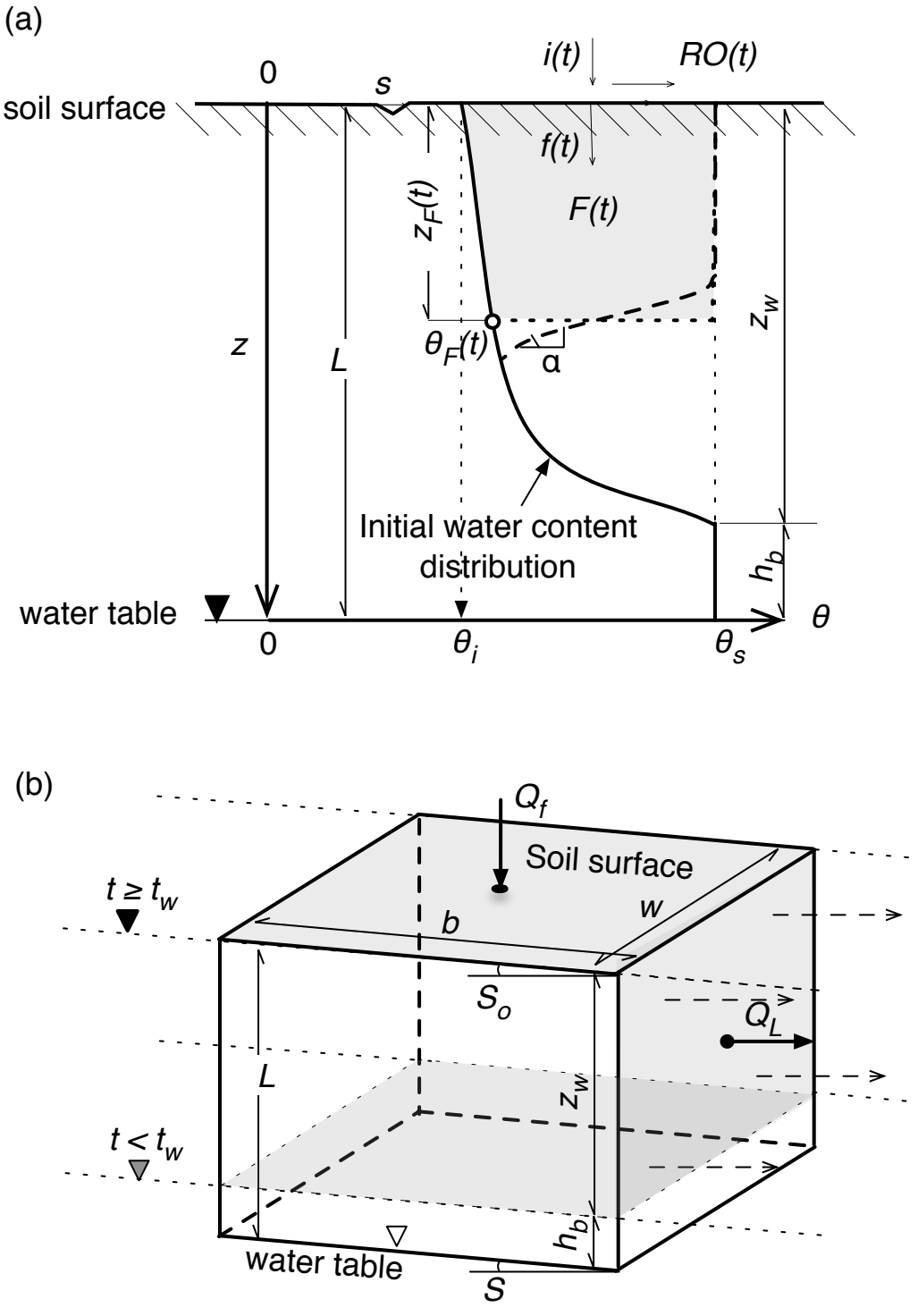
(a)
0
s
i(t)
RO(t)
soil surface
f(t)
F(t)
$z_F(t)$
z_w
z
L
$\theta_F(t)$
α
Initial water content distribution
h_b
water table
0
θ_i
θ_s
θ
(b)
Q_f
Soil surface
$t \geq t_w$
b
w
S_o
Q_L
L
z_w
$t < t_w$
h_b
water table
S

FIG. 1

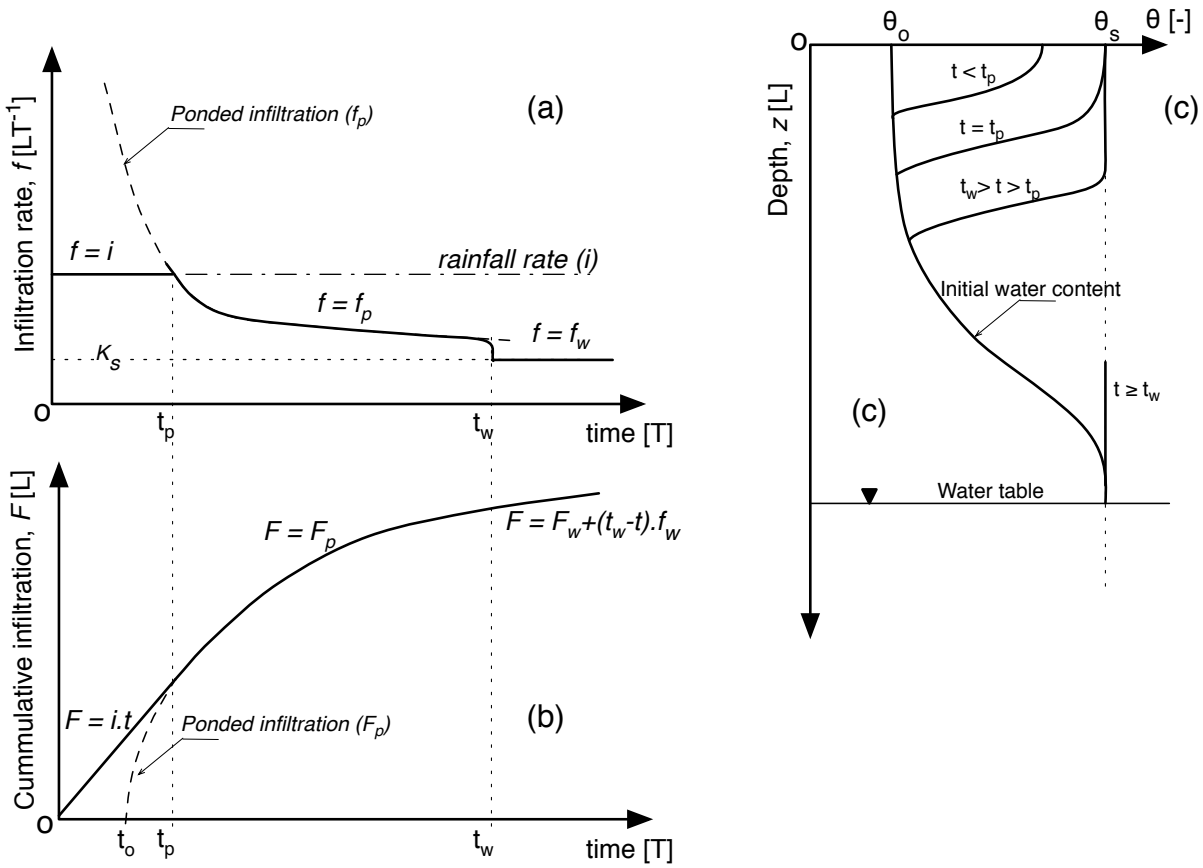
Infiltration rate, f [LT-1]
Ponded infiltration (fp)
(a)
f = i
rainfall rate (i)
f = fp
f = fw
Ks
o
tp
tw
time [T]
Cummulative infiltration, F [L]
F = Fp
F = Fw+(tw-t).fw
F = i.t
Ponded infiltration (Fp)
(b)
to
tp
tw
time [T]
θo
θs
θ [-]
o
Depth, z [L]
t < tp
t = tp
tw> t > tp
Initial water content
(c)
t ≥ tw
(c)
Water table

FIG. 2

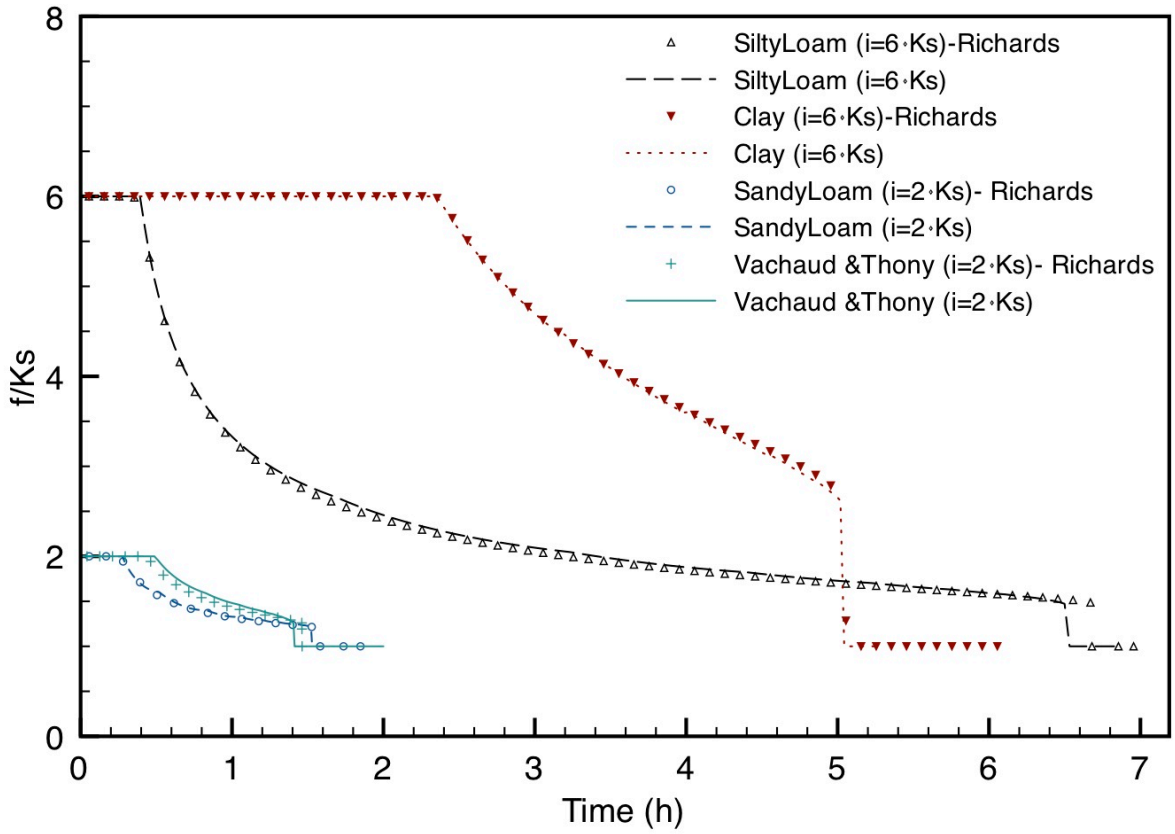
SiltyLoam (i=6·Ks)-Richards
SiltyLoam (i=6·Ks)
Clay (i=6·Ks)-Richards
Clay (i=6·Ks)
SandyLoam (i=2·Ks)- Richards
SandyLoam (i=2·Ks)
Vachaud &Thony (i=2·Ks)- Richards
Vachaud &Thony (i=2·Ks)
f/Ks
Time (h)
0
1
2
3
4
5
6
7
0
2
4
6
8

FIG. 3

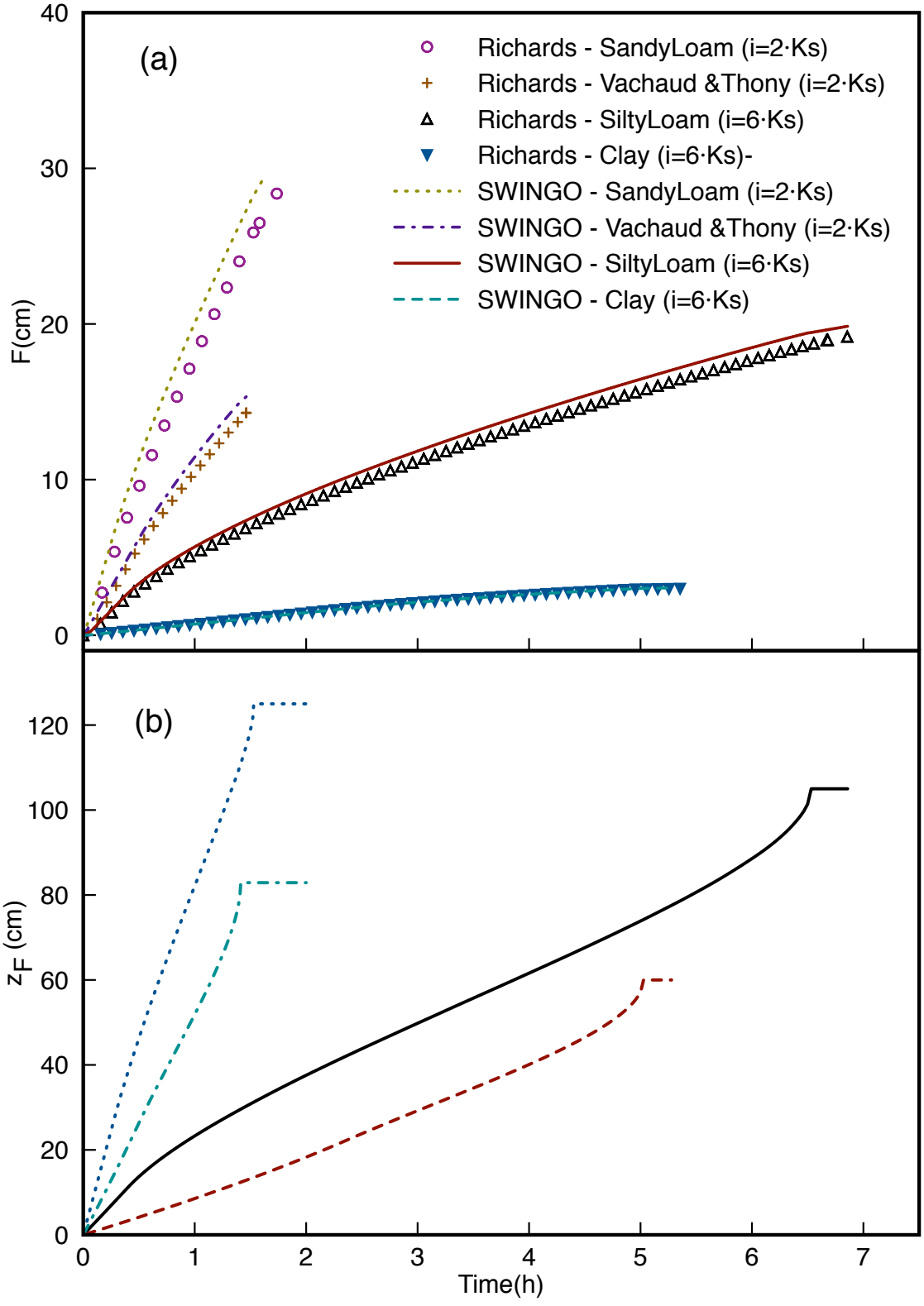
(a)
Richards - SandyLoam (i=2·Ks)
Richards - Vachaud &Thony (i=2·Ks)
Richards - SiltyLoam (i=6·Ks)
Richards - Clay (i=6·Ks)-
SWINGO - SandyLoam (i=2·Ks)
SWINGO - Vachaud &Thony (i=2·Ks)
SWINGO - SiltyLoam (i=6·Ks)
SWINGO - Clay (i=6·Ks)
F(cm)
0
10
20
30
40
(b)
z_F (cm)
0
20
40
60
80
100
120
0
1
2
3
4
5
6
7
Time(h)

FIG. 4

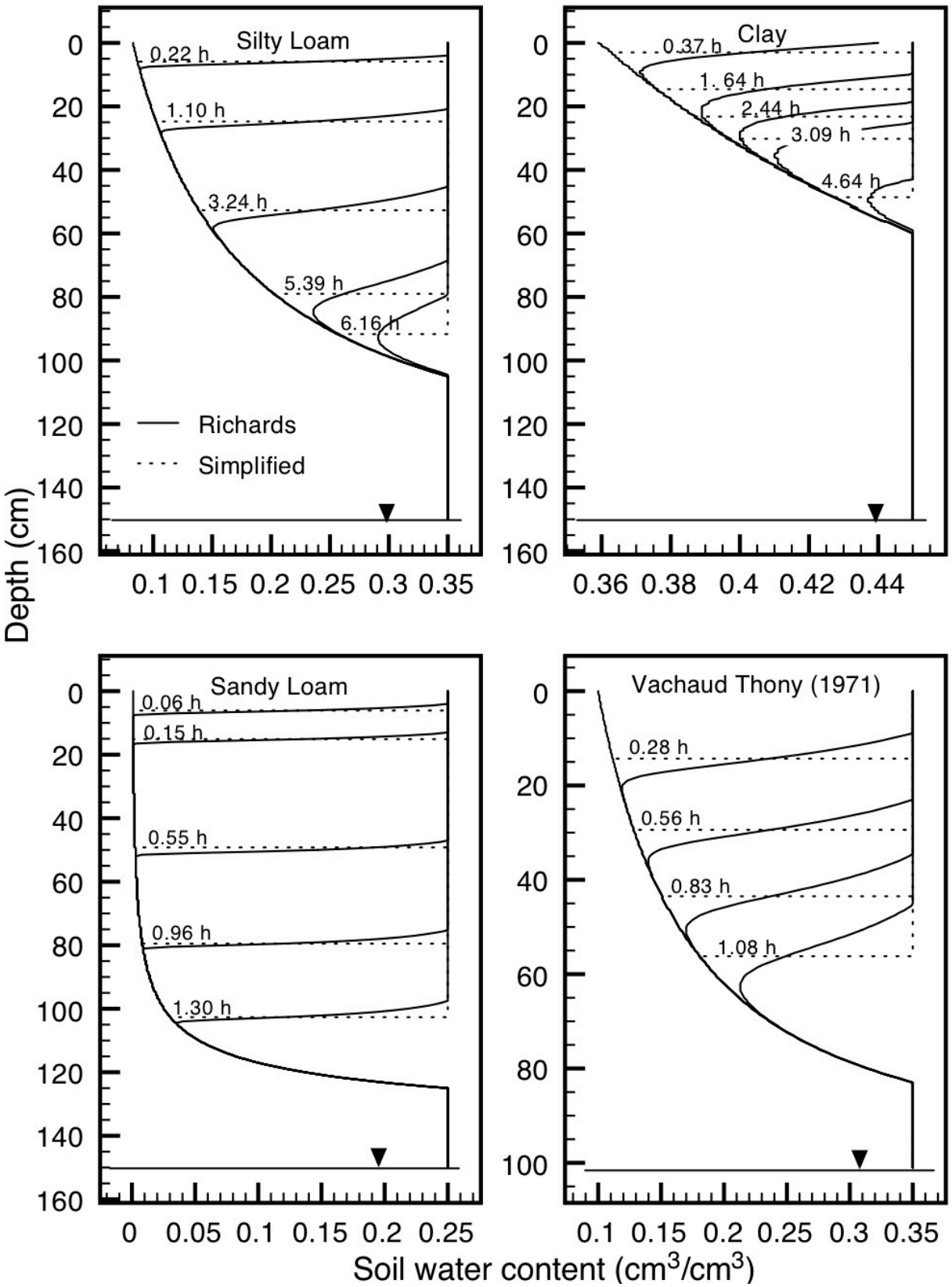
Silty Loam
0.22 h
1.10 h
3.24 h
5.39 h
6.16 h
Richards
Simplified
Clay
0.37 h
1.64 h
2.44 h
3.09 h
4.64 h
Sandy Loam
0.06 h
0.15 h
0.55 h
0.96 h
1.30 h
Vachaud Thony (1971)
0.28 h
0.56 h
0.83 h
1.08 h
Depth (cm)
Soil water content (cm3/cm3)

FIG. 5

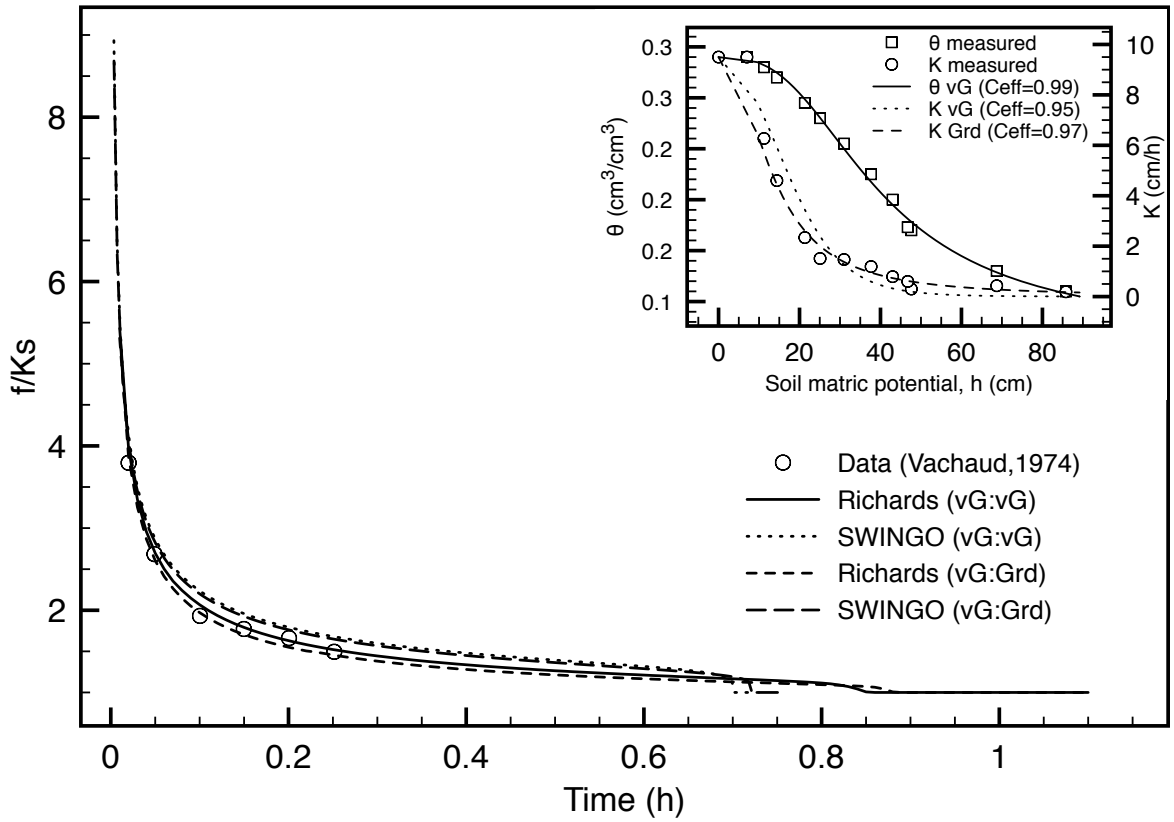
f/Ks
Time (h)
Data (Vachaud,1974)
Richards (vG:vG)
SWINGO (vG:vG)
Richards (vG:Grd)
SWINGO (vG:Grd)
θ measured
K measured
θ vG (Ceff=0.99)
K vG (Ceff=0.95)
K Grd (Ceff=0.97)
θ (cm3/cm3)
K (cm/h)
Soil matric potential, h (cm)

FIG. 6

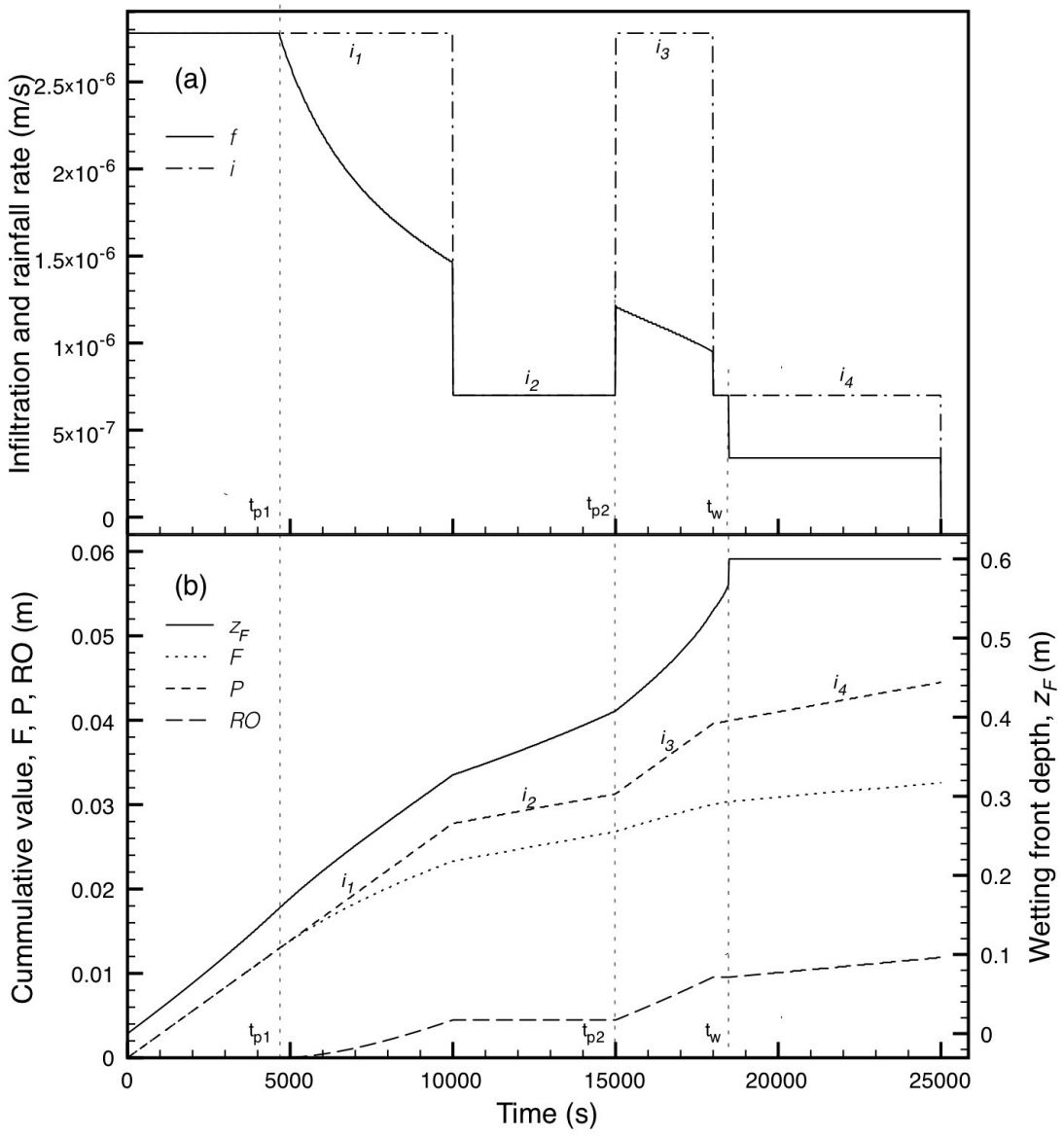
(a)
f
i
i1
i2
i3
i4
tp1
tp2
tw
Infiltration and rainfall rate (m/s)
2.5x10-6
2x10-6
1.5x10-6
1x10-6
5x10-7
0
(b)
ZF
F
P
RO
Cummulative value, F, P, RO (m)
Wetting front depth, zF (m)
0.06
0.05
0.04
0.03
0.02
0.01
0
0.6
0.5
0.4
0.3
0.2
0.1
0
0
5000
10000
15000
20000
25000
Time (s)

FIG. 7

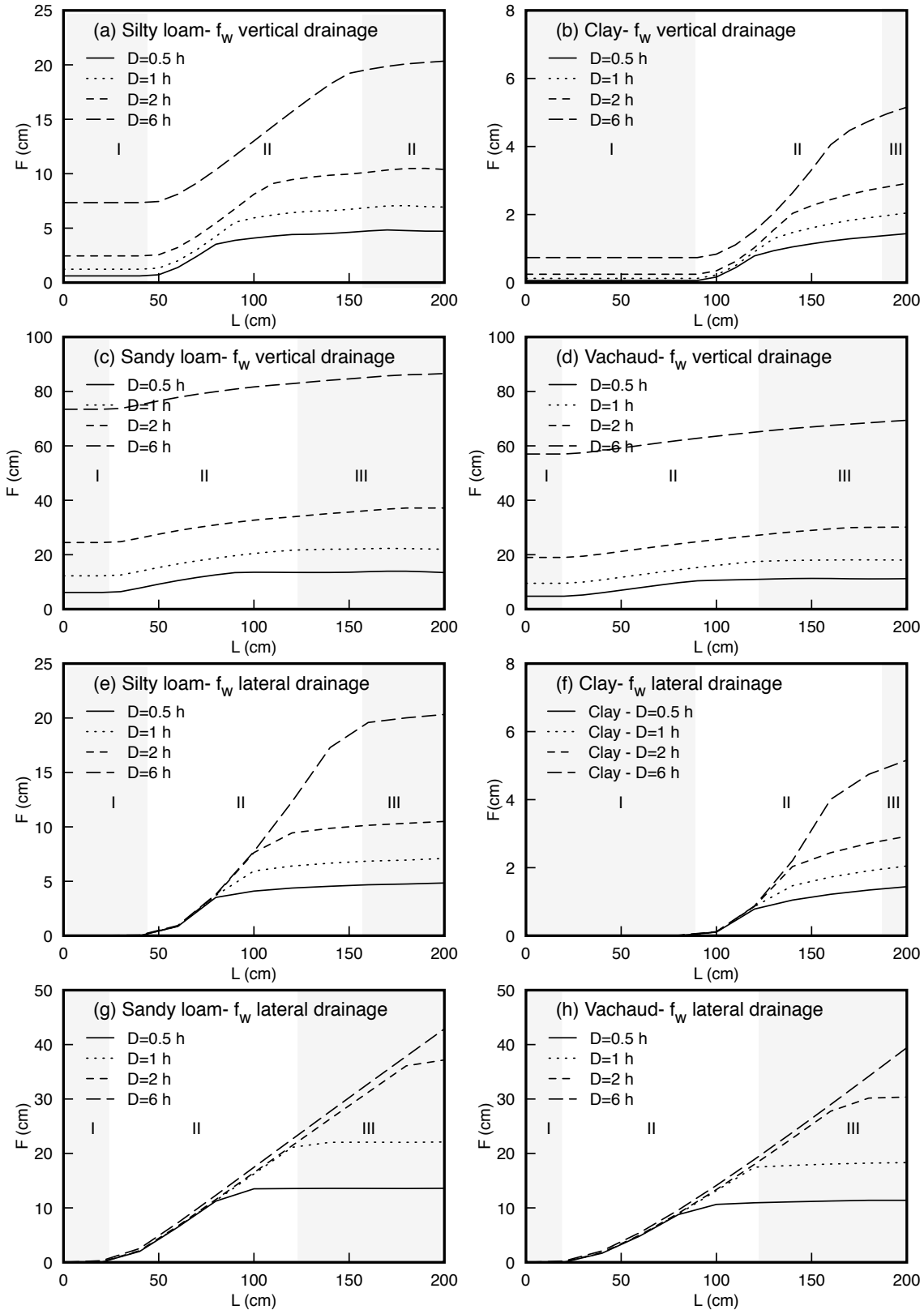
(a) Silty loam- f_w vertical drainage
D=0.5 h
D=1 h
D=2 h
D=6 h
I
II
II
F (cm)
L (cm)
(b) Clay- f_w vertical drainage
D=0.5 h
D=1 h
D=2 h
D=6 h
I
II
III
F (cm)
L (cm)
(c) Sandy loam- f_w vertical drainage
D=0.5 h
D=1 h
D=2 h
D=6 h
I
II
III
F (cm)
L (cm)
(d) Vachaud- f_w vertical drainage
D=0.5 h
D=1 h
D=2 h
D=6 h
I
II
III
F (cm)
L (cm)
(e) Silty loam- f_w lateral drainage
D=0.5 h
D=1 h
D=2 h
D=6 h
I
II
III
F (cm)
L (cm)
(f) Clay- f_w lateral drainage
Clay - D=0.5 h
Clay - D=1 h
Clay - D=2 h
Clay - D=6 h
I
II
III
F(cm)
L (cm)
(g) Sandy loam- f_w lateral drainage
D=0.5 h
D=1 h
D=2 h
D=6 h
I
II
III
F (cm)
L (cm)
(h) Vachaud- f_w lateral drainage
D=0.5 h
D=1 h
D=2 h
D=6 h
I
II
III
F (cm)
L (cm)

FIG. 8

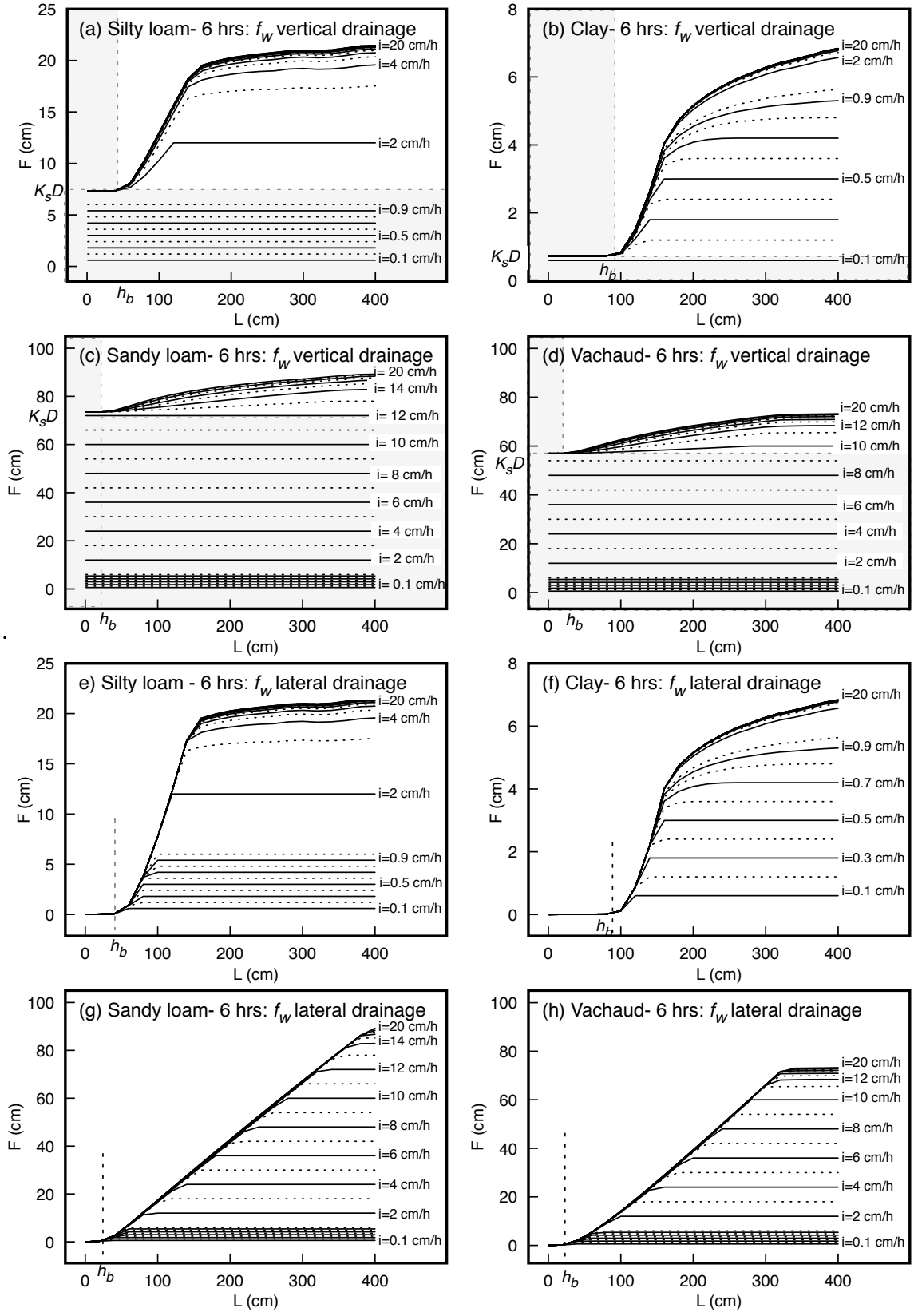
(a) Silty loam- 6 hrs: f_w vertical drainage
i=20 cm/h
i=4 cm/h
i=2 cm/h
i=0.9 cm/h
i=0.5 cm/h
i=0.1 cm/h
K_sD
h_b
F (cm)
L (cm)
(b) Clay- 6 hrs: f_w vertical drainage
i=20 cm/h
i=2 cm/h
i=0.9 cm/h
i=0.5 cm/h
i=0.1 cm/h
K_sD
h_b
F (cm)
L (cm)
(c) Sandy loam- 6 hrs: f_w vertical drainage
i= 20 cm/h
i= 14 cm/h
i= 12 cm/h
i= 10 cm/h
i= 8 cm/h
i= 6 cm/h
i= 4 cm/h
i= 2 cm/h
i= 0.1 cm/h
K_sD
h_b
F (cm)
L (cm)
(d) Vachaud- 6 hrs: f_w vertical drainage
i=20 cm/h
i=12 cm/h
i=10 cm/h
i=8 cm/h
i=6 cm/h
i=4 cm/h
i=2 cm/h
i=0.1 cm/h
K_sD
h_b
F (cm)
L (cm)
e) Silty loam - 6 hrs: f_w lateral drainage
i=20 cm/h
i=4 cm/h
i=2 cm/h
i=0.9 cm/h
i=0.5 cm/h
i=0.1 cm/h
h_b
F (cm)
L (cm)
(f) Clay- 6 hrs: f_w lateral drainage
i=20 cm/h
i=0.9 cm/h
i=0.7 cm/h
i=0.5 cm/h
i=0.3 cm/h
i=0.1 cm/h
h_b
F (cm)
L (cm)
(g) Sandy loam- 6 hrs: f_w lateral drainage
i=20 cm/h
i=14 cm/h
i=12 cm/h
i=10 cm/h
i=8 cm/h
i=6 cm/h
i=4 cm/h
i=2 cm/h
i=0.1 cm/h
h_b
F (cm)
L (cm)
(h) Vachaud- 6 hrs: f_w lateral drainage
i=20 cm/h
i=12 cm/h
i=10 cm/h
i=8 cm/h
i=6 cm/h
i=4 cm/h
i=2 cm/h
i=0.1 cm/h
h_b
F (cm)
L (cm)

FIG. 9